Navigating maritime transition pathways and energy infrastructure towards net zero

Frederik Fristed[1,*], Rasmus Bramstoft[1], Diogo Kramel[2], Lissy Langer[1], Anders Hammer Strømman[2], and Marie Münster[1]

[1]Department of Wind and Energy Systems, Technical University of Denmark, Risø, Denmark
[2]Industrial Ecology Programme, Norwegian University of Science and Technology, Trondheim, Norway
[*]Correspondence: frefri@dtu.dk

Supplemental Information

A Extended results **2**
A.1 Aviation fuel supply . . . 2
A.2 CO_2, electricity and hydrogen infrastructure . . . 3

B Sensitivity analysis **8**
B.1 Onboard carbon capture rates (sensitivity) . . . 8
B.2 Biomass prices (sensitivity) . . . 10
B.3 Global e-fuel import (sensitivity) . . . 12

C Maritime fuel demand **15**
C.1 MariTEAM model . . . 15
C.2 Fuel demand by port and region . . . 16
C.3 Demand growth . . . 17

D Fleet modelling **19**
D.1 Conversion efficiency and emissions of propulsion technologies . . . 19
D.2 Ship-side fuel capacity . . . 20
D.3 Cargo penalty . . . 22
D.4 Onboard carbon capture (OCC) . . . 23
D.5 Retrofitting of legacy fleet . . . 24
D.6 Endogenous tankers . . . 25

E Fuel production pathways **27**

F Regional modelling **29**
F.1 CO_2 storage . . . 29
F.2 Industrial heat demand . . . 31
F.3 Exogenous hydrogen demand . . . 32
F.4 Biomass potential . . . 33
F.5 Capacity based transmission . . . 34

A Extended results

A.1 Aviation fuel supply

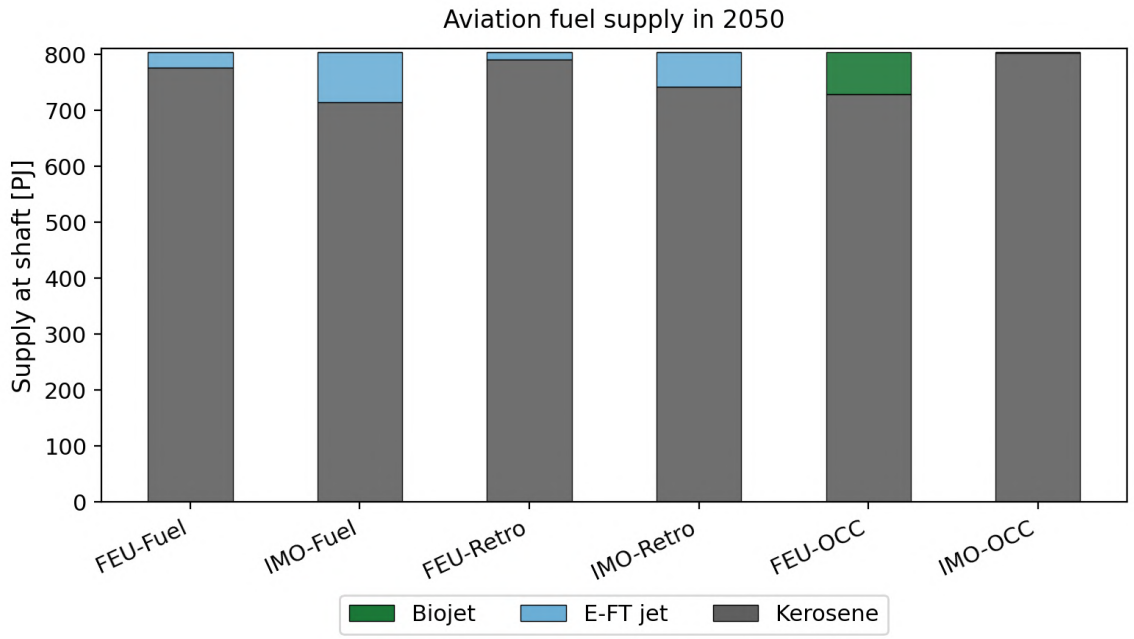

Figure 1: **Aviation fuel supply in 2050 across the six maritime transition scenarios.** Stacked bars show endogenous aviation fuel supply at shaft [PJ]. Unlike the shipping sector, aviation is represented in simplified form without ship-side costs, distance constraints or explicit fleet turnover. Across all pathways, aviation fuel demand remains dominated by fossil kerosene.

A.2 CO_2, electricity and hydrogen infrastructure

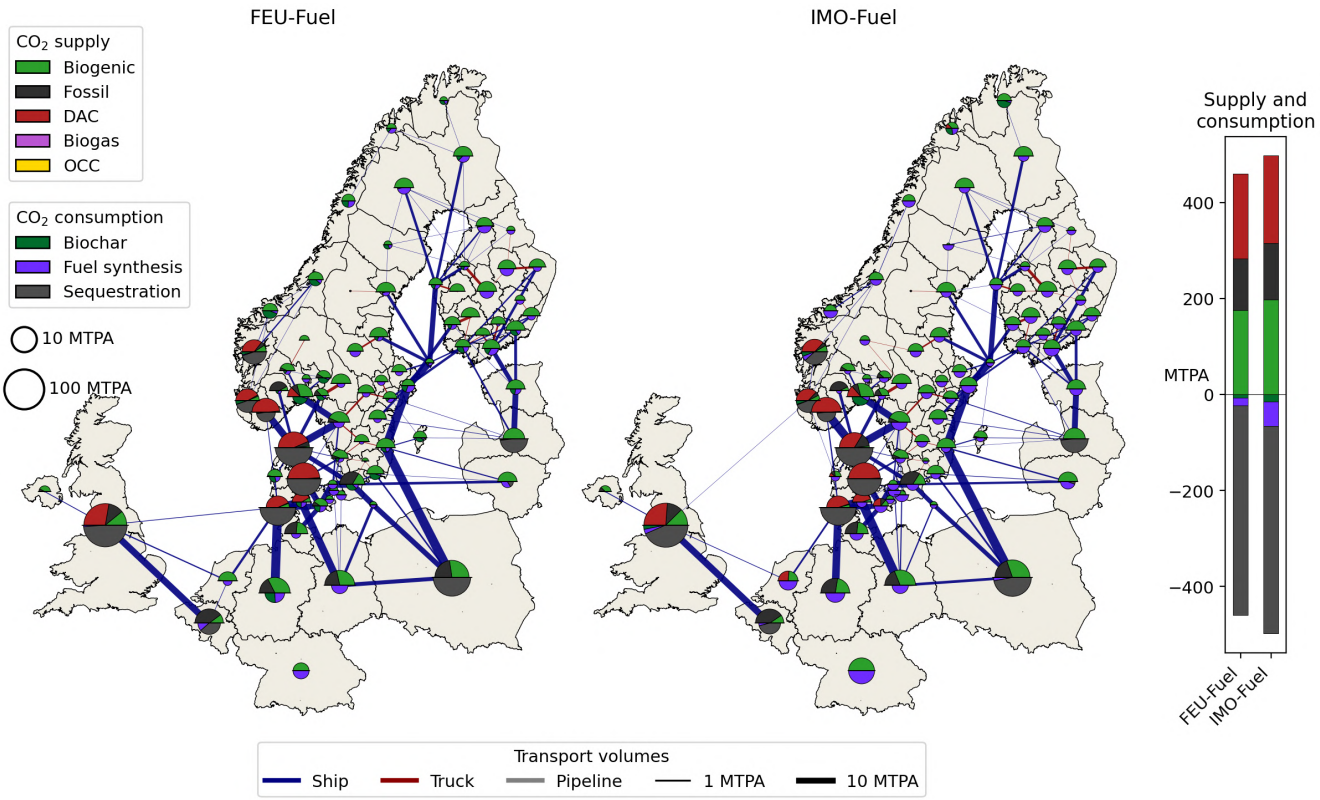

Figure 2: **Spatial distribution of CO_2 capture, utilisation and storage infrastructure under the FEU–Fuel and IMO–Fuel fuel-switching scenarios.** Pie charts show regional CO_2 supply (upper half) and end use (lower half), with all end use determined endogenously.

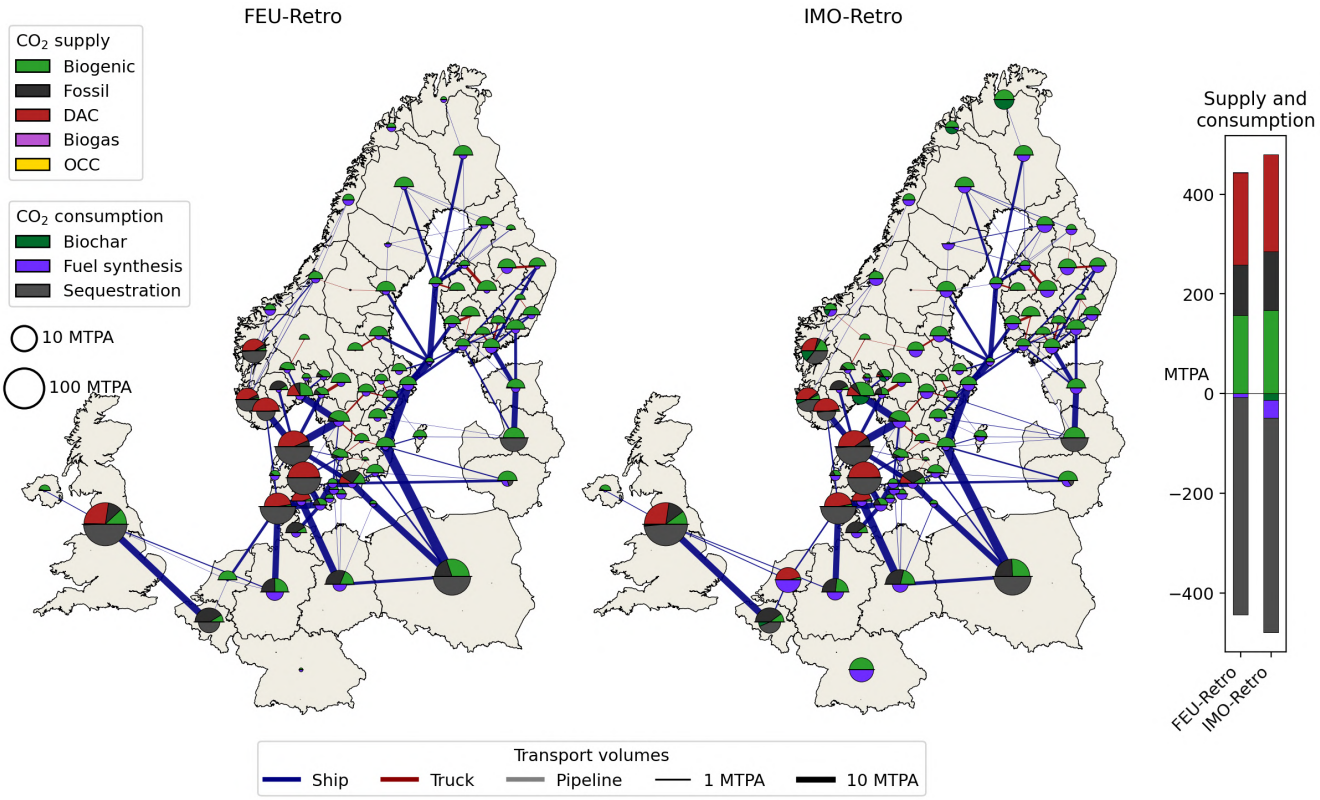

Figure 3: **FEU–Retro** and **IMO–Retro** retrofitting scenarios.

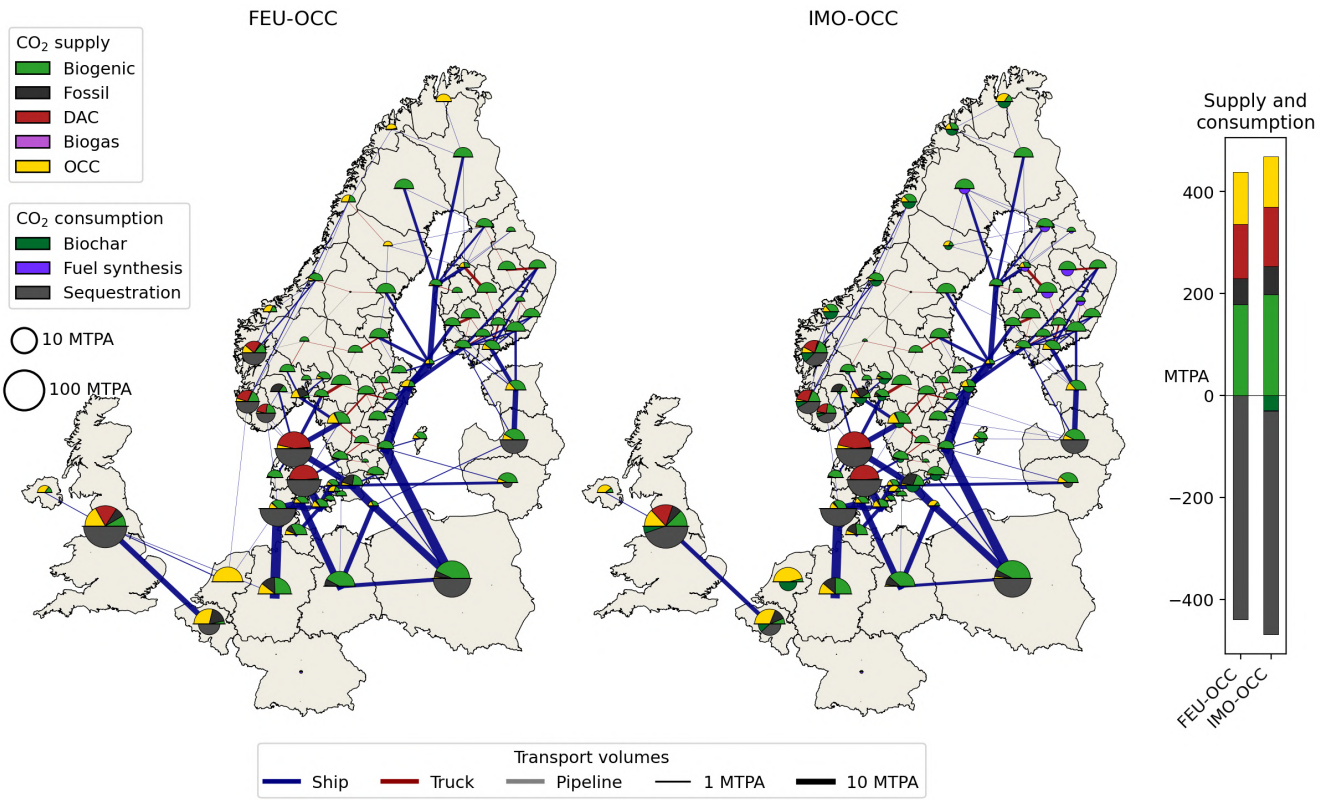

Figure 4: **FEU–OCC** and **IMO–OCC** onboard carbon capture scenarios.

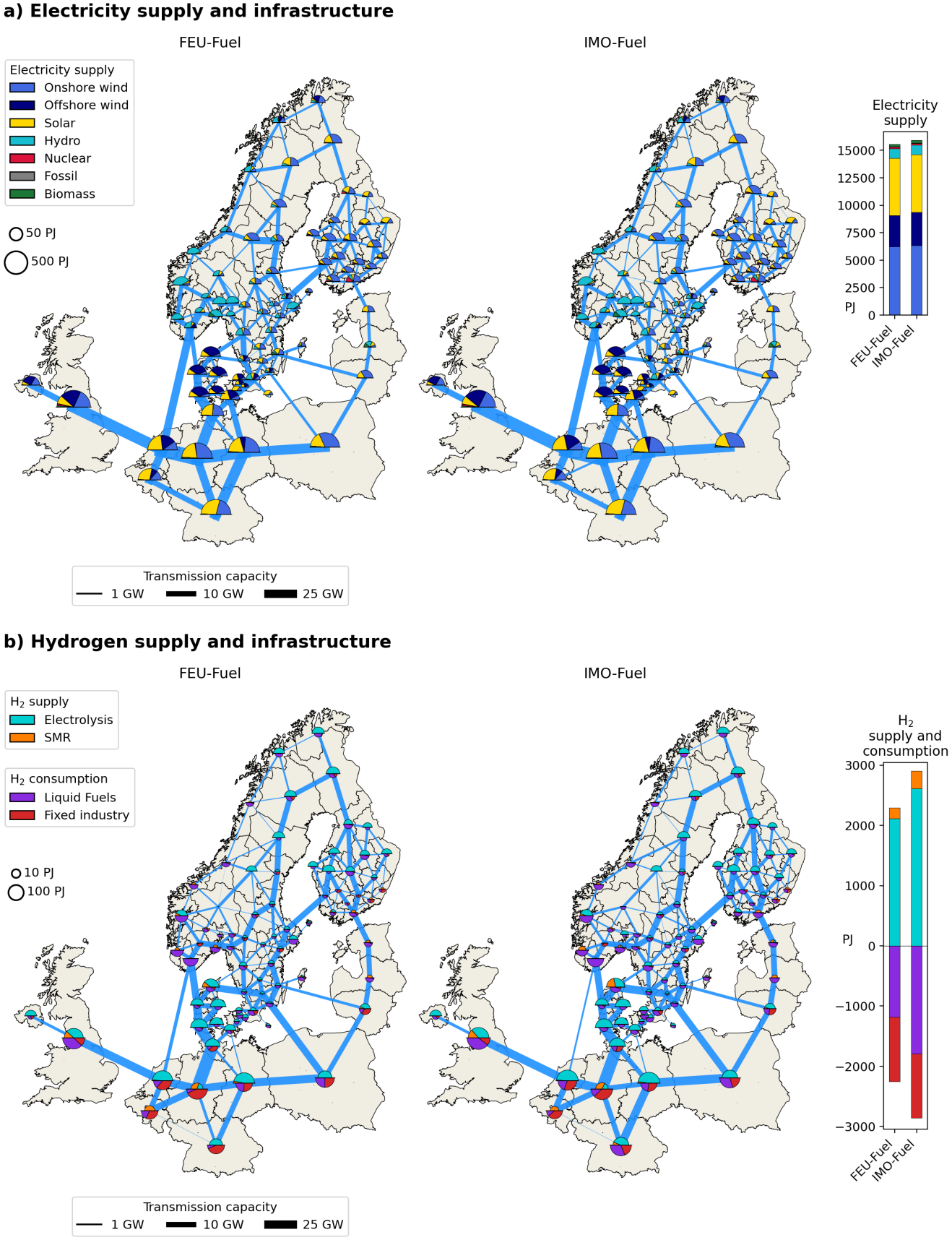

Figure 5: **Electricity and hydrogen infrastructure under the FEU–Fuel and IMO–Fuel fuel-switching scenarios.** (a) electricity generation and transmission capacity. (b) hydrogen production, consumption and pipeline capacity. Pie charts indicate regional supply (upper half) and consumption (lower half).

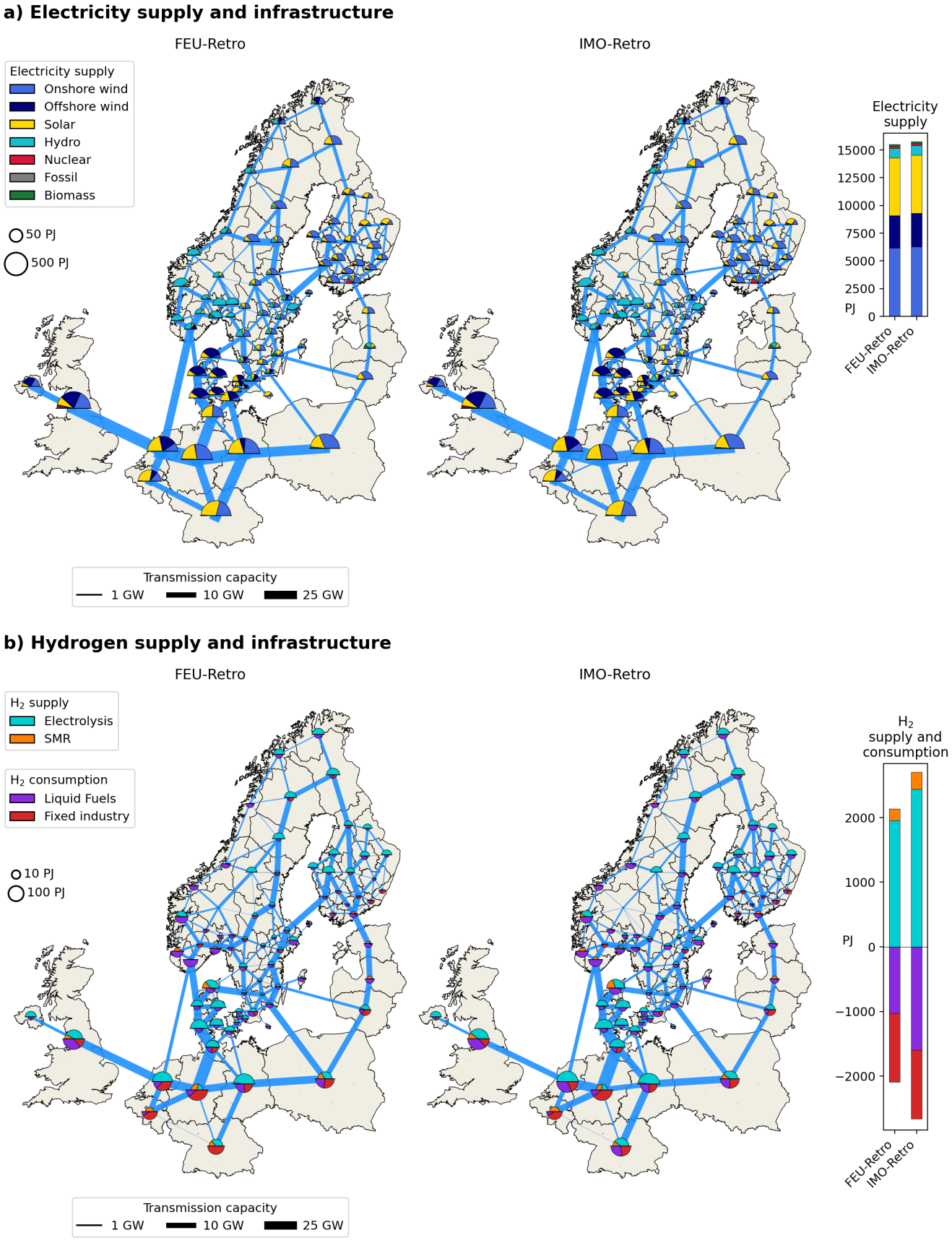

Figure 6: **FEU–Retro** and **IMO–Retro** retrofitting scenarios.

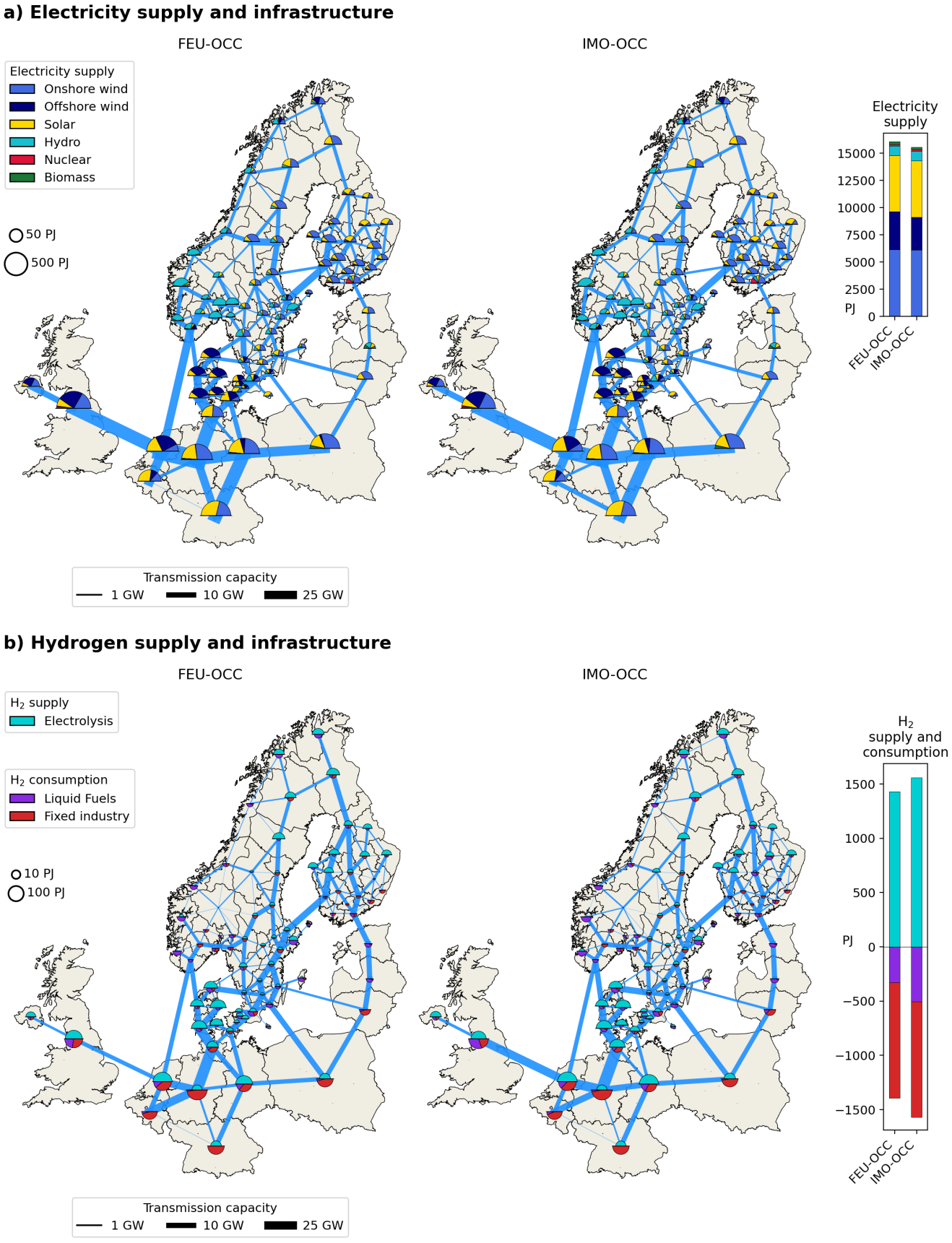

Figure 7: **FEU–OCC** and **IMO–OCC** onboard carbon capture scenarios.

B Sensitivity analysis

B.1 Onboard carbon capture rates (sensitivity)

The performance and cost of onboard carbon capture (OCC) are subject to uncertainty. Key uncertainty parameters include the CO_2 capture rate, the associated fuel penalty and technology cost. We acknowledge that capture rate and fuel penalty are generally correlated, as higher capture rates typically require more energy for separation and compression. However, to keep the sensitivity analysis transparent, we vary only the capture rate, which directly determines the achievable emissions reduction from OCC and therefore strongly affects its feasibility under strict maritime emission constraints (IMO pathways) and its competitiveness in the maritime transition.

We generally assume capture rates of 70% for diesel vessels and 85% for LNG vessels (Supplemental Information D.4). In this sensitivity analysis, we apply a uniform scaling to both capture rates using factors of 0.8× and 0.6× (Table 1), while all other OCC parameters are held constant.

Scale	**Diesel OCC**	**LNG OCC**
	Capture rate [%]	Capture rate [%]
1.0×	70	85
0.8×	56	68
0.6×	42	51

Table 1: **Assumed CO_2 capture rates for OCC**. Baseline capture rates are 70% (diesel) and 85% (LNG). Fuel penalties are held constant at 12% (diesel) and 9% (LNG) across all sensitivity scenarios.

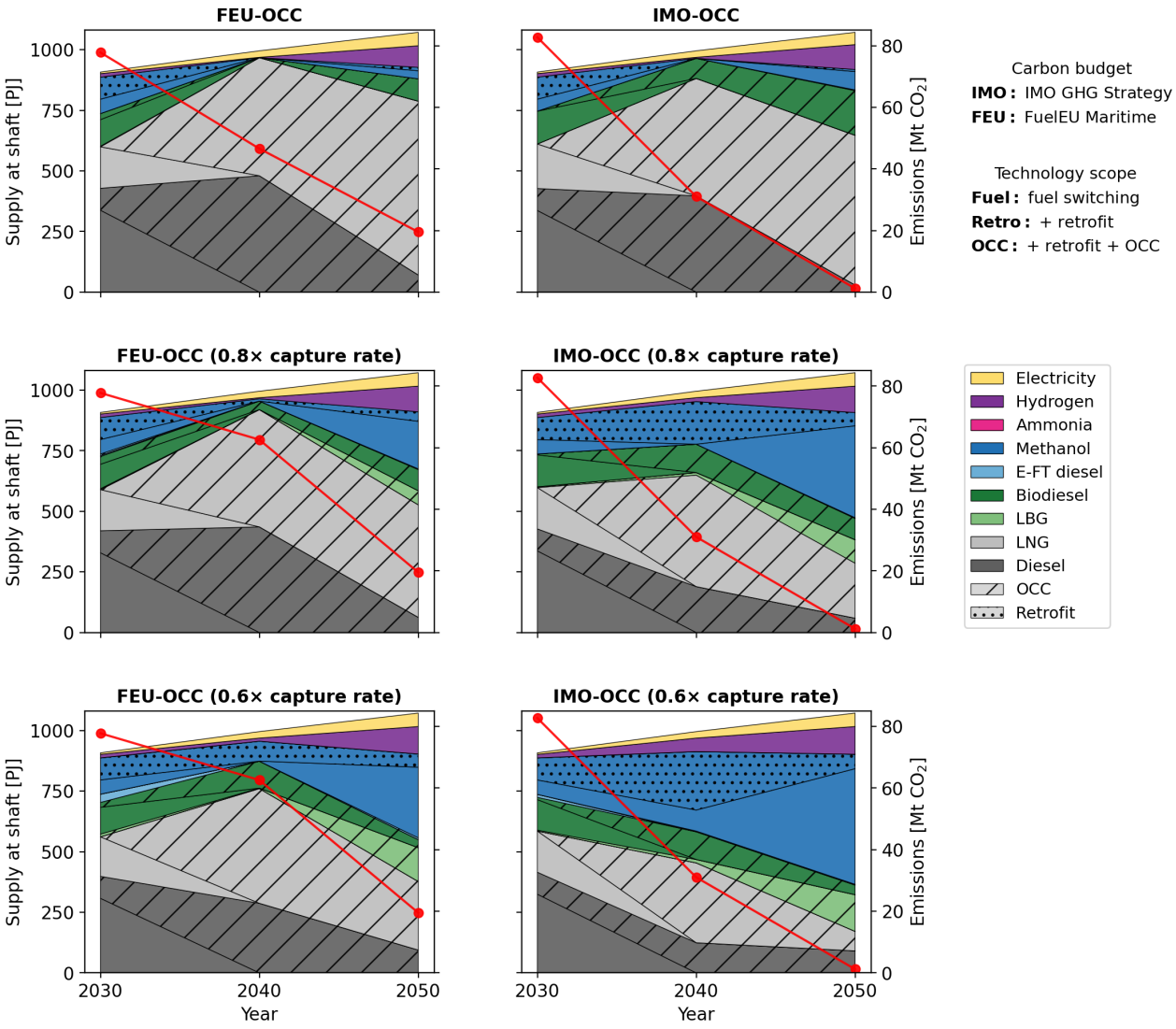

Figure 8: **Maritime fuel supply and greenhouse gas emissions in 2030, 2040 and 2050 under varying onboard carbon capture rates (diesel and LNG OCC) scaled from 0.6×–1× the baseline values.** Stacked areas show annual fuel supply at shaft [PJ] after accounting for conversion efficiency and volumetric cargo penalties. Red lines indicate net maritime greenhouse gas emissions [$MtCO_2e$], including onboard carbon capture. Lower capture rates reduce the overall level of OCC in the fuel mix.

B.2 Biomass prices (sensitivity)

Biomass prices for wood chips and straw are derived from the Danish Energy Agency price projections[1]. These projections reflect long-term market-based biomass supply costs and imply increasing prices over time as biomass demand grows and marginal supply becomes more expensive. We apply these price trajectories in the core maritime transition scenarios. Manure is assigned a fixed price [3.3 €/GJ] and municipal waste is assumed free, reflecting that these streams are primarily treated as local waste resources rather than traded commodities.

However, future biomass prices may increase further due to scarcity and competition with sectors not represented here (e.g. food, chemicals and construction). In this sensitivity analysis, we scale biomass price trajectories from 1× to 2× the baseline values (Table 2). Trajectories are scaled uniformly in 0.2× increments . The constant cost of manure is scaled by the same factor. The IMO-Fuel scenario represents the transition pathway with highest levels of renewable fuel production, and we use this scenario to demonstrate the system response to increasing biomass prices.

Scale	**Straw [€/GJ]**			**Wood chips [€/GJ]**			**Manure [€/GJ]**		
	2030	2040	2050	2030	2040	2050	2030	2040	2050
1.0×	6.4	6.9	7.4	7.1	7.6	8.2	3.3	3.3	3.3
1.2×	7.7	8.3	8.9	8.5	9.1	9.8	4.0	4.0	4.0
1.4×	9.0	9.7	10.4	9.9	10.6	11.5	4.6	4.6	4.6
1.6×	10.2	11.0	11.8	11.4	12.2	13.1	5.3	5.3	5.3
1.8×	11.5	12.4	13.3	12.8	13.7	14.8	5.9	5.9	5.9
2.0×	12.8	13.8	14.8	14.2	15.2	16.4	6.6	6.6	6.6

Table 2: **Price trajectories for tradable solid biomass fuels (straw and wood chips) and manure[1].**

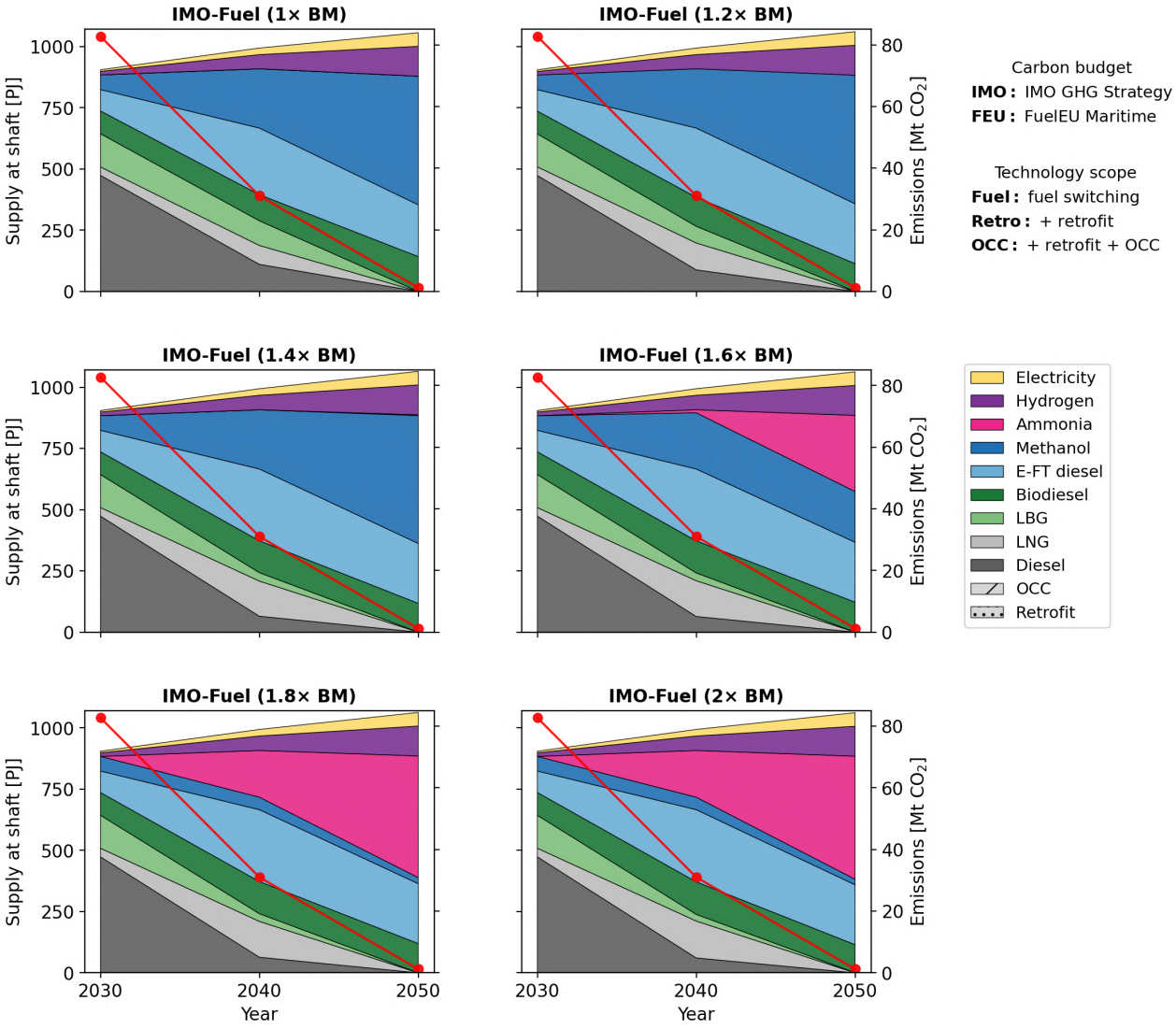

Figure 9: **Maritime fuel supply and greenhouse gas emissions in 2030, 2040 and 2050 under varying prices of tradable solid biomass fuels (straw and wood chips), scaled from 1×–2× the baseline trajectories.** Stacked areas show annual fuel supply at shaft [PJ] after accounting for conversion efficiency and volumetric cargo penalties. Red lines indicate net maritime greenhouse gas emissions [$MtCO_2e$], including onboard carbon capture where applicable. Higher biomass prices shift e-fuel uptake for long-distance shipping from methanol to carbon-free ammonia. This reflects reduced cost competitiveness of pathways relying on biogenic carbon, while leaving fuel supply in other fleet segments largely unchanged.

B.3 Global e-fuel import (sensitivity)

Recent studies suggest that imports of renewable fuels to Europe can be cost-competitive with domestic production under some assumptions[2–4], affecting the scale and location of fuel production and associated infrastructure expansion. In this sensitivity analysis, we introduce a simple representation of global imports of methanol and ammonia. We apply this to the IMO-Fuel pathway, which has the highest levels of renewable fuel production, to test whether imports outcompete domestic production.

Fuel imports are represented as an exogenous buffer from which e-methanol (H_2+CO_2) and e-ammonia (H_2+N_2) can be purchased at fixed prices in 2030, 2040 and 2050. Imports are unlimited and prices are exogenous and inelastic to demand. Cost assumptions are based on the techno-economic assessments by Galimova et al.[2,3], which estimate levelised import costs to Europe (Finland) for supply from Chile (shipping) and Morocco (shipping or pipeline). We compare the central cost assumptions in these studies (7% WACC, medium renewable CAPEX) to the reported lower bound (5% WACC, low renewable CAPEX). For each model year, we select the lowest-cost import option, yielding imports by ship from Chile in 2030 and by ship from Morocco in 2040 and 2050.

Scenario	Fuel	Year	Location	Mode	Cost [€/GJ, LHV]
WACC 7%, CAPEX Medium	Methanol	2030	Chile	Shipping	39.0
WACC 7%, CAPEX Medium	Methanol	2040	Morocco	Shipping	27.4
WACC 7%, CAPEX Medium	Methanol	2050	Morocco	Shipping	23.3
WACC 7%, CAPEX Medium	Ammonia	2030	Chile	Shipping	24.6
WACC 7%, CAPEX Medium	Ammonia	2040	Morocco	Shipping	21.4
WACC 7%, CAPEX Medium	Ammonia	2050	Morocco	Shipping	19.6
WACC 5%, CAPEX Low	Methanol	2030	Morocco	Shipping	30.3
WACC 5%, CAPEX Low	Methanol	2040	Morocco	Shipping	19.7
WACC 5%, CAPEX Low	Methanol	2050	Morocco	Shipping	16.3
WACC 5%, CAPEX Low	Ammonia	2030	Morocco	Shipping	21.1
WACC 5%, CAPEX Low	Ammonia	2040	Morocco	Shipping	16.1
WACC 5%, CAPEX Low	Ammonia	2050	Morocco	Shipping	14.2

Table 3: **Assumed import prices for global e-fuels**[2,3]. For each model year, the lowest-cost supply option across origin and transport mode is selected.

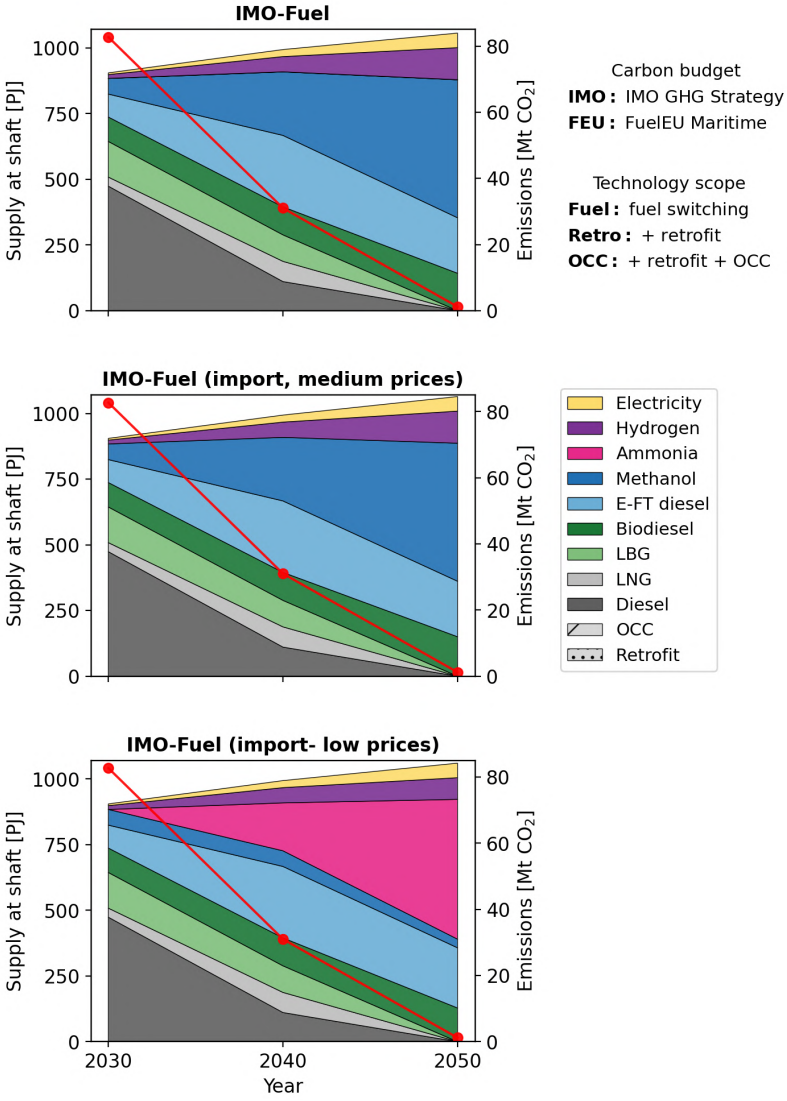

Figure 10: **Maritime fuel supply and greenhouse gas emissions in 2030, 2040 and 2050 under alternative prices for globally traded e-methanol and e-ammonia.** Stacked areas show annual fuel supply at shaft [PJ] after accounting for conversion efficiency and volumetric cargo penalties. Red lines indicate net maritime greenhouse gas emissions [$MtCO_2e$], including onboard carbon capture where applicable. Global imports are only utilised under the lower bound cost assumptions and primarily displace domestic methanol supply for long-distance shipping.

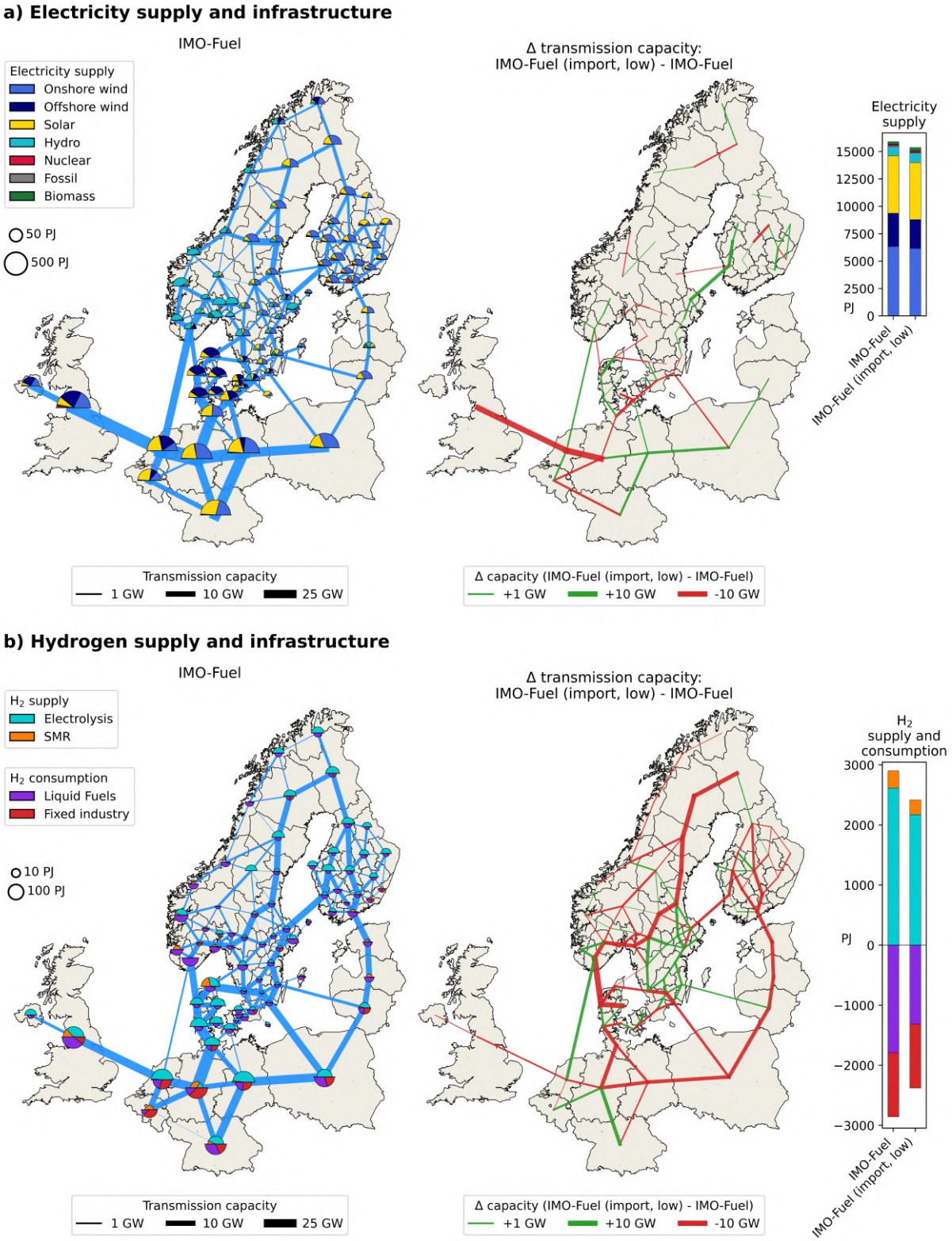

Figure 11: **Spatial distribution of electricity and hydrogen infrastructure under contrasting maritime transition pathways.** Panels show (a) electricity generation and transmission capacity and (b) hydrogen production, consumption and pipeline capacity. Pie charts indicate regional supply (upper half) and consumption (lower half). We compare the IMO-Fuel case without global imports to the medium and lowest cost import cases. Imports of renewable ammonia displace regional hydrogen demand for fuels and reduce the need for electricity and hydrogen transmission, without shifting the decarbonisation burden back to the energy system. Total transmission capacity declines by 3.0% for electricity and 3.0% for hydrogen, relative to the no import case.

C Maritime fuel demand

C.1 MariTEAM model

The MariTeam model (Maritime Transport Environmental Assessment Model) is a bottom-up framework for ship emission assessment that integrates ship positional data with technical vessel specifications and ship resistance models to estimate the energy demand and associated emissions from the shipping sector[5,6].

The model employs Automatic Identification System (AIS) data on ship positions and speed, combined with wind and sea state parameters from ECMWF reanalysis. Technical ship characteristics are obtained from the Sea-web Ships database, with missing parameters estimated following Kim et al. (2022). Ship resistance is evaluated using a meta-model by Kim et al. (2023), integrating calm-water, wind, and wave components. These inputs form the basis for a global inventory of shipping energy demand and emissions. Each vessel is further characterised by parameters such as gross tonnage, utilisation rate, fuel tank size and average voyage time. In this study, we use these data to parameterise fleet modelling, including ownership costs, cargo penalties and onboard carbon capture (OCC). Superscript indices M denote parameters derived from the MariTeam inventory.

We restrict the analysis to voyages to or from Northern European countries (Belgium, Denmark, Estonia, Finland, Germany, Latvia, Lithuania, the Netherlands, Norway, Poland, Sweden and the United Kingdom). Within this scope, the MariTeam model estimates average annual emissions to be 63.5 MtCO_2 in the period 2018–2021.

Ship type	Number of vessels	CO_2e [Mt]	Share of CO_2e [%]
Bulk carriers	5172	7.291	11.485
Chemical tankers	2263	6.689	10.538
Container ships	1886	16.053	25.288
Crude oil tankers	1607	7.024	11.065
Cruise ships	220	4.439	6.993
Gas tankers	756	2.694	4.244
General cargo ships	1650	4.153	6.542
Oil product tankers	368	0.981	1.546
Other activities	24	0.127	0.200
Other service offshore vessels	30	0.093	0.147
Passenger ships	246	5.973	9.409
Refrigerated cargo ships	176	0.991	1.560
Ro-Ro cargo ships	801	6.973	10.984
Total	15199	63.480	100

Table 4: **Inventory of voyages to/from the modelled countries in Northern Europe by ship type (2018–2021)**. Based on data from the MariTEAM model. The table reports CO_2e emissions from domestic shipping and from international voyages affecting the modelled region. For international voyages with either origin or destination in the modelled region, half of the corresponding emissions are included in the shipping sector carbon budget.

C.2 Fuel demand by port and region

Fuel demands at port are determined from the energy demand of voyages, which is split evenly between origin and destination ports. This approach avoids constraining the analysis to today's bunkering hubs, while also expanding the scope to include half of international emissions to and from Europe, consistent with the EU ETS[7], but usually excluded from national emission inventories. Fuel demand is mapped by region, ship type and voyage distance. Nordic regions are represented at NUTS3 level while Northern European countries are modelled at national level (with Germany divided into four regions). Energy demand from the remaining European countries is aggregated under "Rest of Europe" (RoE), while demand from non-European countries is aggregated under "Rest of the World" (RoW).

The 13 ship types in the MariTeam model, shown in Table 4, are grouped into five fleet segments with specific fuel-supply options (Figure 12).

		Newbuilds			
	Legacy				
Fuels	Legacy (all*)	Tanker (fossil)	New long >1500 km	New medium	New short <250 km
Diesel, FT-diesel, biodiesel	■	■	■	■	■
LNG, LBG		■	■	■	■
LPG		■	■	■	■
Methanol			■	■	■
Ammonia			■	■	■
Hydrogen				■	■
Battery electric					■

Transitional technologies	Legacy (all*)	Tanker (fossil)	New long >1500 km	New medium	New short <250 km
Diesel, FT-diesel, biodiesel OCC			■	■	■
Diesel-Methanol retrofit	■	■			
LNG, LBG OCC			■	■	■
LNG-Ammonia retrofit		■			

Figure 12: **Fuel supply options across fleet segments**. Dark cells indicate allowed fuel–segment combinations (f, s). Legacy includes all legacy vessels excluding tankers. Tanker represents vessels transporting fossil oil, gas or chemicals and includes both legacy and newbuild vessels. Tankers transporting renewable fuels are represented endogenously.

C.3 Demand growth

We project future maritime fuel demand using the framework of Kramel et al. (2023), which builds on the gravity model of trade—an established approach for estimating bilateral trade flows between countries as a function of their economic size and distance. The principal explanatory variables in this trade model include gross domestic product (GDP), population and bilateral distance between trading partners. Historical trade data are integrated into the model to calibrate and validate projections, drawing on the CEPII bilateral trade dataset. Further details can be found in Kramel et al. (2024)

To capture long-term structural drivers, the model incorporates Shared Socioeconomic Pathways (SSPs) and Representative Concentration Pathways (RCPs) projections for GDP and population to estimate growth in shipping between pairs of 176 countries with consistent data. These scenarios enable evaluation of alternative trajectories of global trade and associated emissions under varying assumptions of socioeconomic development, climate policies, and technological transitions. Given the substantial role of oil and gas shipments in maritime trade, the model additionally adjusts projections to reflect declining fossil fuel demand under stringent climate mitigation policies for different RCPs. In this study, we adopt SSP2–4.5 as the base scenario, representing a middle-of-the-road pathway.

Energy demand projections are disaggregated into newbuilds (post-2025 vessels) and legacy vessels (pre-2025 vessels). This distinction follows a dynamic stock modelling approach[8], calibrated with data from 200,000 operational and decommissioned vessels. A technical ship lifetime of 30 years is assumed, implying that most of today's fleet will be retired and replaced by 2050. The transition to certain low- and zero-carbon fuels, including methanol, ammonia, hydrogen and battery electric propulsion, is restricted to newbuilds, except for fuel retrofitting which is allowed in certain transition scenarios.

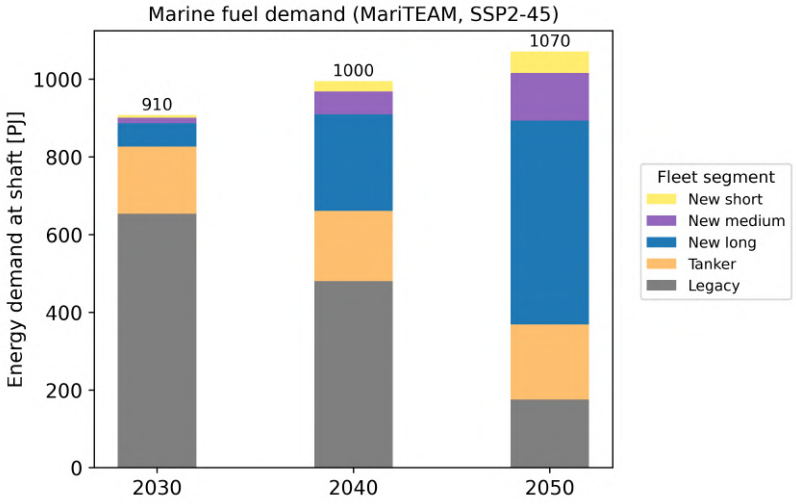

Figure 13: **Final energy demand at shaft [PJ] across modelled fleet segments**. Fleet segments are defined by vintage (legacy/newbuild) and distance (short < 250 km, medium, long > 1500 km). Demand is shown as aggregated across al countries but modelled by region.

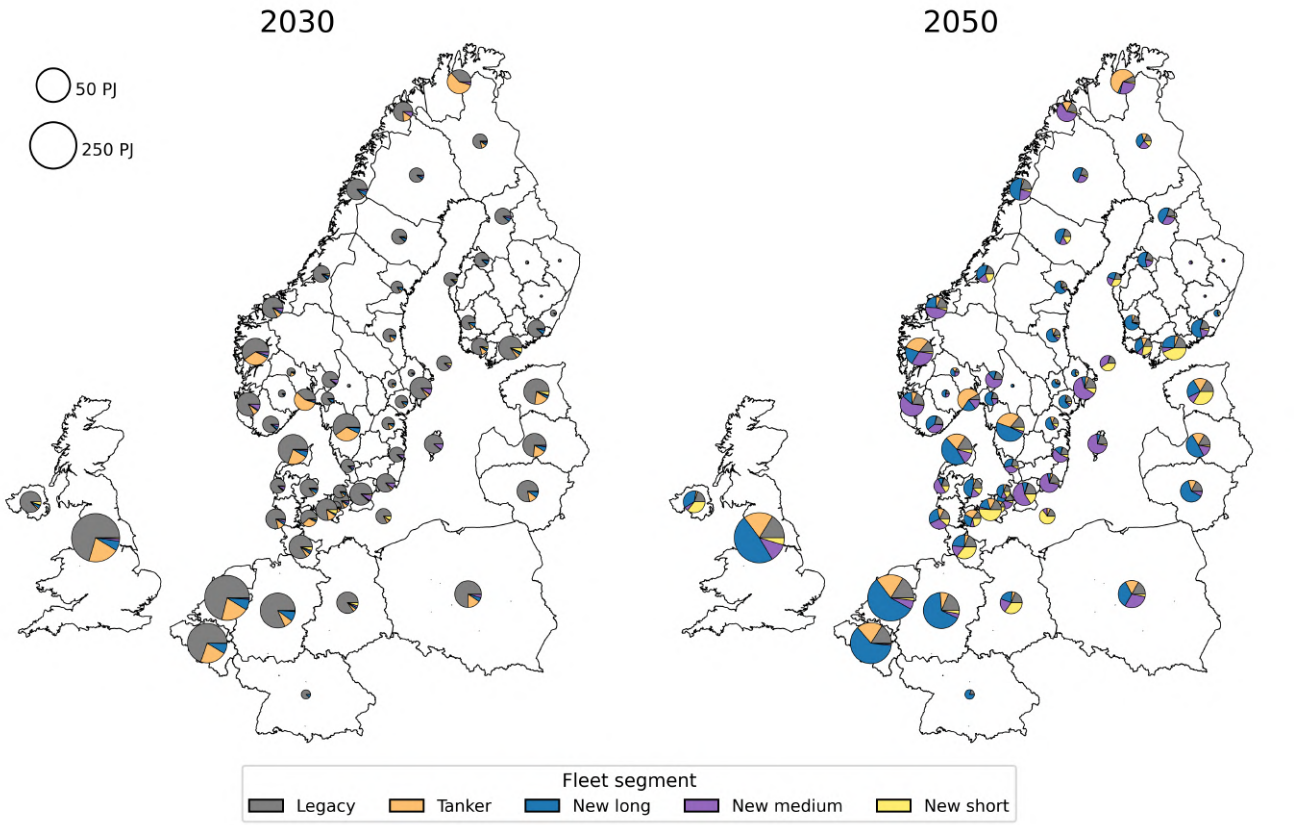

Figure 14: **Spatial distribution of maritime energy demand at shaft in 2030 and 2050 across the modelled fleet**. Fleet segments are defined by vintage (legacy vs. newbuild) and distance (short < 250 km, medium 250–1500 km, long > 1500 km). Demand is modelled by region.

D Fleet modelling

D.1 Conversion efficiency and emissions of propulsion technologies

Energy demand is expressed as shaft power and converted to fuel demand using technology-specific conversion efficiencies (Table 5). Since constant efficiencies are applied for 2030–2050, we assume comparable efficiencies for mature fossil engine technologies (diesel and LNG) and ICE-based e-fuel pathways (methanol, ammonia and hydrogen) to enable a consistent comparison of fuel options across the time horizon. We assume 45 % efficiency for methanol, ammonia and hydrogen ICEs. While ammonia ICEs currently operate around 35 %, efficiency is expected to improve over time[9], and assuming the same efficiencies avoids biasing fuel pathway in 2050 based on today's performance. Fuel cell (FC) propulsion achieves higher conversion efficiencies than ICE systems, but at higher investment and operating costs. Battery electric (BE) propulsion achieves very high efficiency but is limited to newbuild vessels on short-distance routes ($<$ 250 km).

Emissions are accounted for on a well-to-wake basis, including fuel production, transport and onboard combustion, while embodied emissions from ships and infrastructure are excluded. Values are largely adapted from Kramel et al.[10]. We include direct onboard CO_2 emissions and CO_2e emissions from methane slip, hydrogen slip and direct nitrous oxide emissions, as well as process-related emissions such as fugitive methane emissions during extraction. For biogas used in liquefied biogas (LBG) pathways, we assume 1% leakage during production.

Engine	Fuel	Efficiency [%]	Direct emissions [tCO_2/GJ]	Process emissions [tCO_2e/GJ]
ICE	Diesel	50	0.0775	0.00126
ICE	FT-diesel	50	0	0.00119
ICE	Biodiesel	50	0	0.00115
ICE	LNG	50	0.0572	0.00749
ICE	LBG	50	0	0.01369
ICE	Methanol	45	0	0
ICE	Ammonia	45	0	0
ICE	Hydrogen	45	0	0.00077
FC	Hydrogen	65	0	0
FC	Ammonia	60	0	0
FC	Methanol	50	0	0
BE	Electricity	95	0	0

Table 5: **Energy conversion efficiency and emission factors for engine technologies and fuel types.** Direct emissions represent direct CO_2 emissions from onboard combustion. Process emissions represent other greenhouse-gas emissions associated with fuel use, such as non-CO_2 emissions during combustion, fuel slip at the engine and fugitive emissions during fuel production.

D.2 Ship-side fuel capacity

The cost of ship-side fuel capacity is expressed per unit of rated capacity [M€/GJ hr^{-1}], indexed by fuel type, fleet segment and region. The model therefore represents regional capacity to handle each fuel rather than investments in individual vessels. Costs are derived for each fuel and fleet segment (f, s) from the techno-economic assessment of Korberg et al.[11], including only capital and operating expenditures for propulsion and storage. We exclude hull costs and operational expenses such as maintenance, insurance and crew, assuming that any fuel-specific differences, including those that may occur for renewable options in the early stages of adoption, are negligible compared with fuel costs. All costs are benchmarked to 2030 and applied unchanged through 2050, which may overstate the relative cost of emerging options compared with mature liquid hydrocarbon internal combustion engines.

For the propulsion system, capital costs c_f^{prop} and fixed operating costs o_f^{prop} are annualised using a 4 % discount rate and technology lifetimes[11]. Within each fleet segment, the mean utilisation rate (UR_s^M) is applied as a scaling factor. This reflects that ships with lower utilisation rates face greater exposure to the cost of propulsion capacity. For example, a short-sea vessel operates around 6200 h/yr compared to 7000 h/yr for long-distance vessels.

$$OC_{f,s}^{M,\text{prop}} = \frac{c_f^{\text{prop}} \cdot CRF_f^{prop} + o_f^{\text{prop}}}{UR_s^M} \tag{1}$$

The fuel storage system is sized based on the mean voyage duration within each fleet segment (VL_s^M). This reflects that ships with long range requirements face greater exposure to the cost of fuel storage capacity.

$$OC_{f,s}^{M,\text{sto}} = c_f^{\text{sto}} \cdot VL_s^M \tag{2}$$

Fleet segment	FLH [hr yr^{-1}]	Utilisation	Voyage duration [hr]
Legacy	6870	0.78	140
Tanker	6990	0.80	145
Long distance	6990	0.80	145
Medium distance	6850	0.78	105
Short distance	6200	0.71	15

Table 6: **Mean full-load hours, utilisation rate and voyage duration by fleet segment.** Data is from the MariTEAM inventory. Within each fleet segment, values are mean values weighted by each ship's share of total demand.

Fuel	**Legacy** *(all*)*	**Tanker** *(fossil)*	**New long** *>1500 km*	**New medium** *<1500 km*	**New short** *<250 km*
Diesel (ICE)	0.166 / 4 200	0.163 / 4 100	0.169 / 4 200	0.164 / 4 100	0.180 / 4 500
Diesel + OCC	0.191 / 14 400	0.188 / 14 300	0.195 / 14 400	0.189 / 14 300	0.205 / 14 700
LNG (ICE)		0.273 / 12 200	0.335 / 15 000	0.254 / 11 300	0.276 / 12 400
LNG + OCC		0.298 / 22 400	0.361 / 25 200	0.279 / 21 500	0.301 / 22 600
Methanol (ICE)			0.191 / 4 800	0.180 / 4 500	0.198 / 4 900
Methanol (FC)			0.524 / 30 900	0.519 / 31 100	0.572 / 34 300
Methanol retrofit	0.137 / 4 500	0.135 / 4 900			
Ammonia (ICE)			0.238 / 10 700	0.215 / 9 700	0.236 / 10 600
Ammonia (FC)			0.592 / 35 000	0.575 / 34 500	0.633 / 38 000
Ammonia retrofit		0.135 / 10 700			
Hydrogen (ICE)				0.258 / 11 500	0.277 / 12 400
Hydrogen (FC)				0.388 / 23 000	0.420 / 25 100
Electricity (BEV)					0.246 / 7 600

Table 7: **Ship-side capacity costs for propulsion and onboard storage systems**. Based on Korberg et al.[11]. Values show overnight capital cost [M€/GJ/hr] and annual fixed O&M costs [€/GJ/hr].

D.3 Cargo penalty

Renewable fuels generally have lower volumetric energy densities than fossil counterparts. While drop-in options such as Fischer-Tropsch diesel or bio-oil perform comparably to diesel, fuels like methanol, ammonia, liquefied biogas (LBG) and liquid hydrogen (LH_2) require larger fuel tanks to maintain range. For all fuel options, the reduction in volumetric energy density relative to diesel exceeds the gravimetric; we therefore assume ships are volume-constrained. We assume constant maritime service demand, so displaced payload is offset by increased fleet activity.

For each fuel–segment pair (f, s), we apply a cargo penalty (CP) representing the capacity loss. Here, ρ_f is the volumetric energy density of fuel f relative to diesel, and α_s^M is the weighted mean value of the fuel-tank share of gross tonnage for segment s, derived from the MariTeam model. Additionally, we account for displaced volume from storing captured CO_2 with onboard carbon capture. The cargo penalty varies by fuel and fleet segment (f, s), ranging from 0 % for drop-in fuels to 17.9 % for hydrogen (LH_2) in medium-distance newbuild vessels (< 1500 km). All values are provided in Table 8. Currently, ships not operating on fixed routes often carry oversized fuel tanks, enabling bunkering at low-cost locations. Thus, it is case specific whether lower volumetric energy density will actually reduce cargo capacity.

$$CP_{f,s} = \frac{\alpha_s \left(1 - \frac{1}{\rho_f}\right)}{1 - \alpha_s} \tag{3}$$

Fuel (f)	Legacy	Tanker	New long	New medium	New short
Diesel, E-FT-diesel, biodiesel	0.0	0.0	0.0	0.0	0.0
Diesel (OCC)	5.7	4.0	6.6	5.6	4.4
LPG	–	1.1	1.8	1.5	1.2
LNG, LBG	–	1.3	2.2	1.9	1.5
LNG (OCC)	–	4.1	6.9	5.9	4.6
Methanol	–	2.6	4.4	3.8	3.0
Ammonia	–	4.3	7.2	6.2	4.9
LH_2	–	12.6	–	17.9	14.1
Battery electric	–	–	–	–	10.0

Table 8: **Cargo penalty [%] across fleet segments (s) and fuels (f).**

Batteries are treated separately since the energy density of batteries is still improving compared to liquid fuels, and recent studies emphasise that electrified ships must account for both weight and volume constraints of the battery and electric motor when designing[12,13]. We apply a generic cargo penalty of 10% to battery electric propulsion, consistent with the battery's share of deadweight observed on recent electric ferries. We note that battery electric propulsion is deployed across all maritime transition scenarios for short-sea transport.

For fuels used together with onboard carbon capture, captured CO_2 is liquefied and stored onboard. We assume a storage density of $\rho_{LCO_2} = 1070$ kg m^{-3} (at $-30\,^{\circ}$C and 13 barg), consistent with the values reported in the EverLoNG project[14]. When calculating the cargo penalty, the effective volumetric energy density is adjusted to account for the additional tank volume required for storing liquid CO_2.

D.4 Onboard carbon capture (OCC)

Onboard carbon capture (OCC) for diesel- and LNG-fuelled engines is modelled as monoethanolamine (MEA) post-combustion capture with flue-gas heat integration[15]. Capture efficiency is assumed at 70 % for diesel engines and 85 % for LNG engines. The associated fuel penalties are implemented as efficiency losses of 12 % and 9 %, respectively, consistent with recent assessments of onboard solvent capture systems[14,16,17].

Dispatch of fossil fuels with onboard carbon capture produces residual emissions, making OCC technologies incompatible with strict net-zero accounting unless these emissions are offset. Captured fossil CO_2 is returned to the modelled CO_2 grid, from which it may be transported for permanent storage (CCS) or utilised as feedstock in e-fuel production (CCU). When renewable fuels are used with OCC, such as biodiesel or e-FT-diesel in diesel-OCC engines or liquefied biogas (LBG) in LNG-OCC engines, the captured emissions are treated as net negative once permanently stored because the captured CO_2 originates from biogenic or atmospheric sources.

Capital and operating costs for OCC are derived from Visonà et al.[17], which provides techno-economic estimates for large-scale capture systems on container vessels based on fuel throughput and a fixed CO_2 capture fraction of exhaust emissions. Capital costs include the capture unit, compression, onboard CO_2 storage and auxiliary equipment. Fixed operating costs are applied as 3 % of capital cost to represent maintenance, while variable operating costs include solvent replacement. Additional fuel consumption due to capture is treated endogenously as an efficiency penalty in the model. We adopt the intermediate unloading scenario, in which captured CO_2 is discharged at every second port call, and apply a single representative cost per unit of fuel consumption across the fleet. To account for both the fuel penalty and the cargo penalty, the net emission abatement from OCC $\eta_{f,s}^{\text{net}}$ can be expressed as:

$$\eta_{f,s}^{\text{net}} = 1 - (1 - \eta_f)(1 + FP_f)(1 + CP_{f,s}), \tag{4}$$

where η_f is the capture rate of fuel f, FP_f the fuel penalty, and $CP_{f,s}$ the cargo penalty for fuel f in segment s. Table 10 summarises the net CO_2 reduction for diesel and LNG OCC, accounting for capture rates, fuel penalty and cargo penalty. The fuel penalty reflects additional energy use for capture, while the cargo penalty reflects lost cargo capacity due to space requirements for liquefied CO_2. Together, these penalties increase fuel demand per unit final energy at shaft.

Parameter	Diesel	LNG	Unit
Investment cost	67.5	60.5	k€/GJ/h
Operating cost (incl. solvent)	2430	2430	€/GJ/h/yr

Table 9: **Cost parameters for onboard carbon capture (OCC) used in the energy system model[17].**

Fuel (f)	Capture rate [%]	With fuel penalty [%]	With fuel and cargo penalty [%]
Diesel OCC	70	66.4	64.5
LNG OCC	85	83.7	82.7

Table 10: **Net CO_2 reduction for OCC technologies**. Values are shown for long-distance newbuild vessels ($>$1500 km). Because the cargo penalty scales with the relative size of a vessel's fuel tank, this represents the upper bound across fleet segments.

D.5 Retrofitting of legacy fleet

Retrofitting costs are expressed as a 25% increase relative to the total newbuild cost of a conventional diesel-fuelled vessel of the same class, consistent with the upper bound of current industry estimates[18–20]. We assume that propulsion and fuel storage systems account for 30% of total ship capital expenditure[21,22]. Thus, retrofitting costs are represented as an additional 83% of the propulsion and storage costs of a standard vessel, providing a consistent proxy across fleet segments. The technology is restricted to conversions from diesel to methanol dual-fuel and from LNG to ammonia dual-fuel propulsion, reflecting technologies currently available or nearing commercial readiness. Fixed operating costs follow the retrofitted fuel and propulsion system.

$$OC_{f,\mathrm{s}}^{M,\mathrm{retro}} = \left(1 + \frac{0.25}{0.30}\right) \cdot \left(OC_{\mathrm{Diesel},s}^{M,\mathrm{prop}} + OC_{\mathrm{Diesel},s}^{M,\mathrm{sto}}\right) \tag{5}$$

Retrofitting is applied only to the legacy fleet. The technology remains at an early stage, and both costs and lead times are highly uncertain. Because of this immaturity, we impose a ramping limit of 10% of legacy demand in 2030. Thereafter, retrofitting potential is only limited by the unretired share of the fleet, represented through a survival curve (Table 11), based on the technical lifetime and age distribution of ships in the MariTEAM dataset (Figure 15).

Segment, fuel	Unit	2030	2040	2050
Legacy (all*), diesel	%	61.8	36.2	6.6
Tanker, diesel	%	78.0	42.7	9.9
Tanker, LNG	%	80.0	50.6	13.6

* Excluding tankers transporting fossil oil, gas and chemicals.

Table 11: **Unretired Share of the 2025 legacy fleet in each model year**. Based on a 30-year technical lifetime and the age distribution of vessels in the MariTEAM dataset.

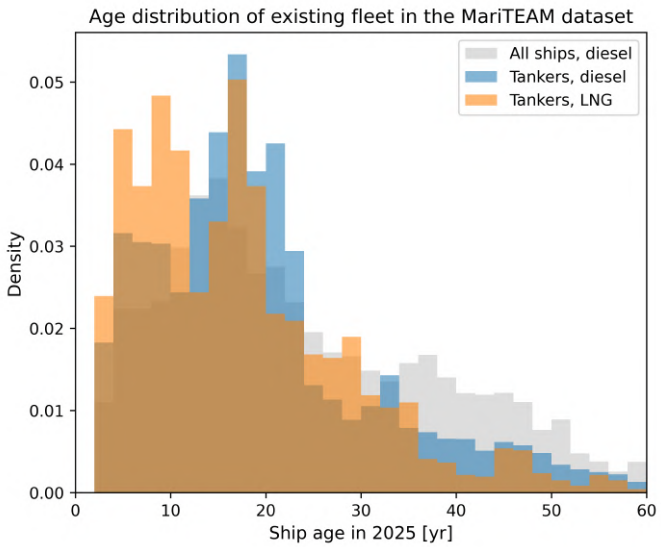

Figure 15: **Age distribution of the legacy fleet in the MariTEAM dataset.**

D.6 Endogenous tankers

Liquid fuels and CO_2 can be transported by tanker ships. We parameterise endogenous bulk shipping for five tanker classes: liquid hydrocarbons (LHC), methanol, ammonia, liquefied hydrogen (LH_2) and liquefied CO_2 (LCO_2). Storage and handling requirements differ across classes and determine both cost and energy use (Table 12–13).

Energy intensity. To align tanker energy use with MariTEAM ship types, we use oil tankers as proxies for liquid hydrocarbons, chemical tankers for methanol and gas tankers for ammonia, hydrogen and CO_2. This is a simplification, particularly for LH_2 carriers, where dedicated studies indicate higher boil-off and energy consumption than LNG-type carriers[23,24]. Despite this optimistic assumption, our results show negligible deployment of hydrogen tankers. For each tanker class t and route between origin and destination (o, d), we compute energy intensity as the ratio of total energy use to total cargo transport, normalised by mean route distance:

$$EI^{M}_{t,o,d} = \frac{\sum_{i=1}^{n} E_{i,t,o,d}}{(\sum_{i=1}^{n} C_{i,t,o,d})\, D_{o,d}}. \tag{6}$$

We then compute an average energy intensity by tanker for each tanker EI^{M}_{t} weighting individual routes by the share of transported cargo. The corresponding fuel penalty for fuel f is defined using the lower heating value LHV_f:

$$FP^{M}_{t,f} = \frac{EI^{M}_{t}}{LHV_f}. \tag{7}$$

This assumes that renewable-fuel tankers are powered by the fuel they transport, consistent with current industry practice for oil and gas tankers. For CO_2 transport, we apply the same procedure, assuming CO_2 tankers are powered by fossil diesel.

Transport cost. We represent endogenous shipping as a bulk transport service rather than modelling investment in tanker vessels. Transport costs are parameterised by (i) a bulk-dependent term C^{M}_{W} [€/GJ] and (ii) a distance-dependent term C^{M}_{D} [€/GJ·km]:

$$C_{t,o,d} = C^{M}_{W} + C^{M}_{D} \cdot D_{o,d}. \tag{8}$$

Capital costs, fixed operating costs and port fees are based on Korberg et al.[11], annualised with a 30-year technical lifetime and 4 % discount rate. Following their methodology, tanker utilisation from MariTEAM (6990 FLH/yr), service speed (26 km/h) and port time (48 h/roundtrip) are used to allocate costs between time at sea and time at port. Port fees and the port-time share of capital and fixed operating costs define C^{M}_{W}, while time at sea defines C^{M}_{D}.

Tanker class	LHV [GJ/m^3]	Energy intensity [GJ/m^3/km]	MariTeam proxy	Fuel penalty [GJ/GJ/km]
LHC	35.8	$2.47{\cdot}10^{-4}$	Oil tanker	$6.90{\cdot}10^{-6}$
Methanol	15.8	$1.46{\cdot}10^{-4}$	Chemical tanker	$9.23{\cdot}10^{-6}$
Ammonia	12.7	$2.88{\cdot}10^{-4}$	Gas tanker	$2.26{\cdot}10^{-5}$
LH_2	8.5	$2.88{\cdot}10^{-4}$	Gas tanker	$3.38{\cdot}10^{-5}$
LCO_2	–	$6.33{\cdot}10^{-4}$ [GJ/t/km]	Gas tanker	–

Table 12: **Energy intensity and fuel penalty for endogenous tankers**. Tankers transport liquid hydrocarbons (LHC), methanol, ammonia, liquefied hydrogen (LH_2) and liquefied CO_2 (LCO_2).

Tanker class	Bulk cost C_W [€/GJ]	Distance cost C_D [€/GJ·km]	Emissions [kgCO_2/GJ]
LHC	0.0490	$2.26{\cdot}10^{-5}$	–
Methanol	0.106	$4.98{\cdot}10^{-5}$	–
Ammonia	0.182	$1.36{\cdot}10^{-4}$	–
LH_2	0.184	$1.98{\cdot}10^{-4}$	–
LCO_2	52.97 [€/t]	$3.10{\cdot}10^{-2}$ [€/t/km]	$4.68{\cdot}10^{-5}$

Table 13: **Cost and emission parameters for endogenous tankers.**

E Fuel production pathways

Fuel production pathways in OptiFlow are modelled as a network, where nodes represent conversion processes and arcs represent feedstock and energy flows. Pathways are defined by sequences of inputs and outputs through these processes, governed by conversion efficiencies (Figure 16) and techno-economic parameters (Table 14). We model endogenous investments in fuel production capacity, including investment costs and fixed and variable operating costs.

Fuel	**Production pathway**	**Investment cost** [M€/GJ h^{-1}]	**Fixed O&M cost** [€/GJ h^{-1} yr^{-1}]	**Variable cost** [€/GJ]
Shipping fuels				
FT-diesel	H_2 + CO_2	0.266	13300	0.62
FT-diesel	Straw, wood	0.258	7700	0.33
HTL-diesel	Manure	0.430	20400	7.13
HPO-diesel	H_2 + straw	0.270	13300	7.13
LBG[a]	Manure, straw	0.0943	3300	11.2
Methanol	H_2 + CO_2	0.241	7200	-
Methanol	H_2 + straw, wood	0.431	11500	-
Methanol	H_2 + biogas	0.609	24400	1.84
Ammonia	H_2	0.240	7200	-
Aviation fuels				
FT-kerosene	H_2 + CO_2	0.266	13300	0.620
FT-kerosene	Straw, wood	0.258	7700	0.330

[a] Costs include biogas production in manure-based digestion tanks but not manure feedstock.

Table 14: **Cost assumptions for renewable fuel production pathways in 2050**[25,26]. Investment costs are overnight costs expressed per unit of fuel production capacity. Fixed O&M are annualised. Variable costs exclude feedstock costs, which are modelled endogenously. Reported values correspond to 2050; all technologies follow exogenous learning trajectories between 2030 and 2050.

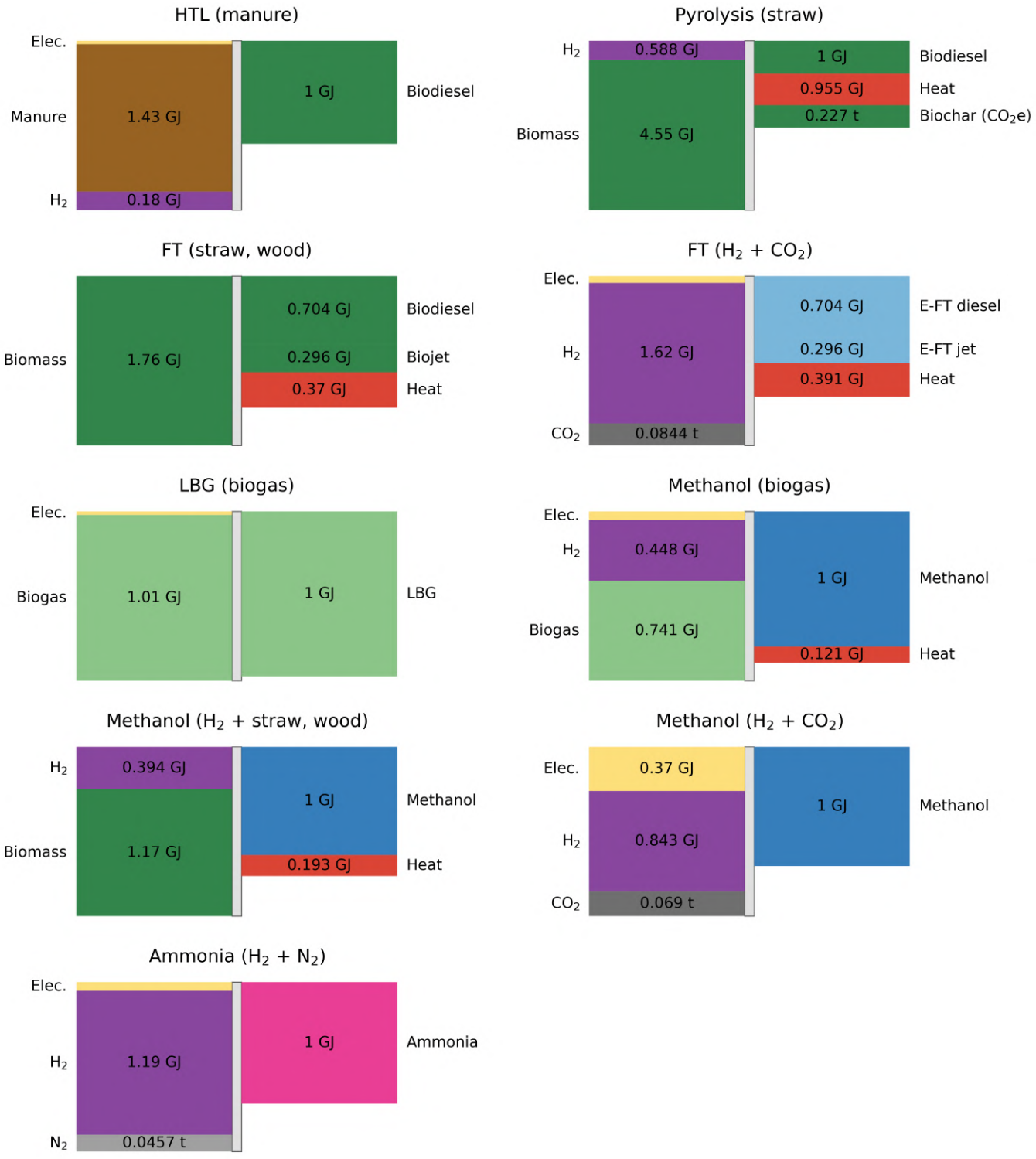

Figure 16: **Renewable fuel production pathways represented in OptiFlow**[25,26]. Diagrams illustrate the conversion relationships between energy and feedstock inputs, fuel outputs and co-products. All energy flows are normalised to 1 GJ net fuel output. Mass-based streams [t] are displayed using a fixed visual scaling factor of 3 relative to energy flows [GJ]. Hydrothermal liquefaction (HTL) and pyrolysis pathways include upgrading via hydrogenation to maritime fuels-grade products. The straw fast pyrolysis pathway co-produces liquid biofuel, heat and biochar, where biochar is credited as negative emissions assuming 80% sequestration over 100 years.

F Regional modelling

F.1 CO_2 storage

Regional CO_2 storage potentials are derived from the JRC CO2StoP database[27], which reports site-level storage capacities for European saline aquifers and depleted hydrocarbon reservoirs. The database compiles national assessments that differ in scope, methodology and geological detail. To obtain consistent estimates, reported technical capacities are converted to dynamic (pressure-limited) capacities using storage efficiency factors[28,29]. A factor of 0.02 is applied to saline aquifers without hydrocarbon fields and 0.06 to depleted hydrocarbon reservoirs. Units already based on dynamic simulation or detailed site characterisation were left unscaled. Scaled storage capacities are annualised assuming a 53.5-year fill period, yielding a total injection potential of 600 $MtCO_2\,yr^{-1}$ in Europe and 440 $MtCO_2\,yr^{-1}$ within the modelled regions, most of which are located in the North Sea area of Denmark, Norway and the United Kingdom. These values are in the same range as the 450 $MtCO_2\,yr^{-1}$ projected by the European Commission[30], although that estimate covers only the European Union and excludes non-EU regions such as Norway and the United Kingdom.

Storage capacities are aggregated to the model's regions (Figure F.1). Each storage unit is assigned to a region by spatial intersection with onshore polygons. Units whose centroids do not intersect onshore regions are classified as designated offshore areas. For storage units assigned to onshore regions, injection is assumed to occur at the model node, represented by the region centroid, consistent with the treatment of other energy system resources. Offshore units are represented as spatially distinct injection points, requiring CO_2 transport from the associated onshore region via ship or pipeline. Offshore injection points correspond to the capacity-weighted centroid of all offshore storage areas aggregated to the same onshore model region.

At regional scale, the distinction between onshore and offshore storage is not always clear, as storage formations may extend across coastal boundaries. In some cases, such as Denmark, storage capacity located predominantly offshore by volume is represented as onshore in the regional aggregation. Given this limitation, injection costs are applied uniformly across all storage resources. Cost assumptions are based on offshore storage estimates at large-scale injection rates of approximately 5 $Mt\,CO_2\,yr^{-1}$ [31], providing a consistent and conservative representation of storage costs while keeping spatial detail in CO_2 transport and infrastructure.

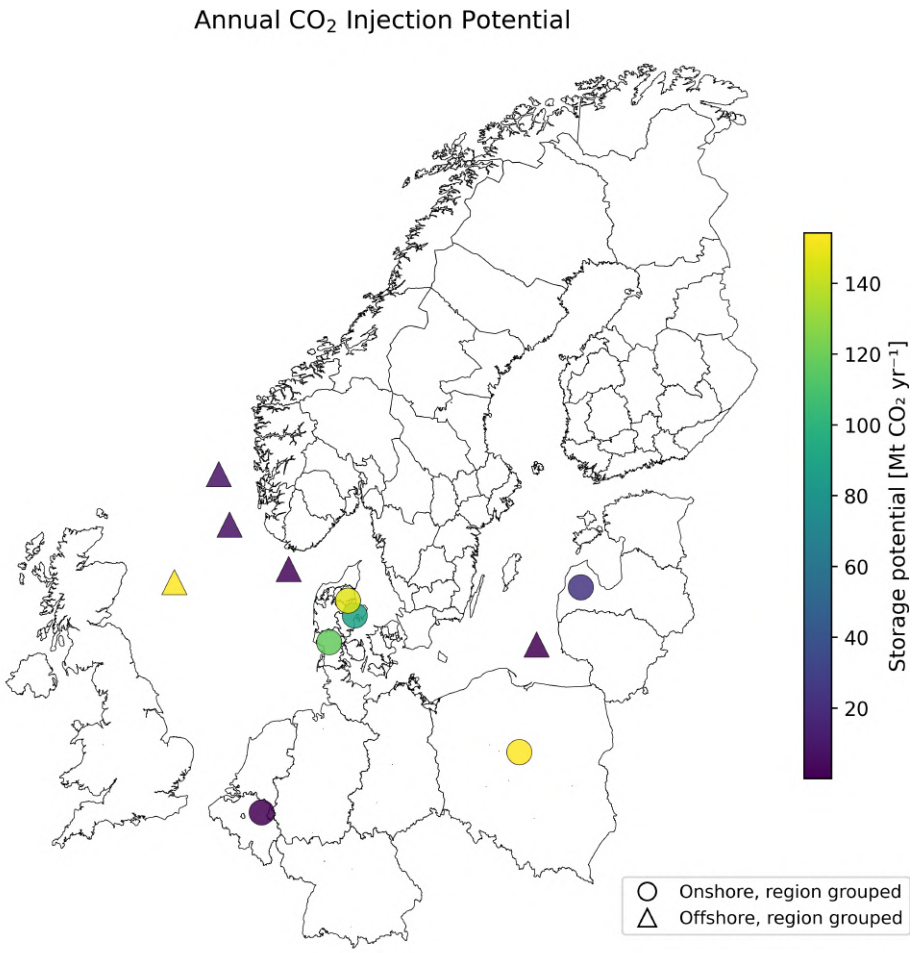

Figure 17: Annual CO_2 injection potentials across model regions.

F.2 Industrial heat demand

Industrial electricity and heat demands are derived from Rehfeldt et al.[32], which provide country-level industrial activity by subsector and process together with process-specific energy demand for electricity, space heat, and process heat split into three temperature levels (low $< 100°$C, medium 100–$500°$C, and high $> 500°$C). We aggregate these data to obtain national industrial heat demand by temperature level for the subsectors iron and steel, non-ferrous metals, pulp and paper, non-metallic minerals, basic chemicals and food and beverage.

Regional demands are obtained by spatially disaggregating national subsector demands using facility-level CO_2 emissions reported under EU ETS or E-PRTR[33]. For each country and subsector, facilities are assigned a share of the national heat demand equal to their share of subsector emissions. This allocation is applied uniformly across temperature bins, such that each facility receives the same fraction of low-, medium- and high-temperature demand. Facilities are then mapped to the model regions using GIS overlay.

In the model, industrial heat demands are met by fuels and conversion technologies, and associated CO_2 point-source emissions are endogenously determined by fuel use. Emissions are classified as fossil or biogenic according to the carbon content of the supplied fuels.

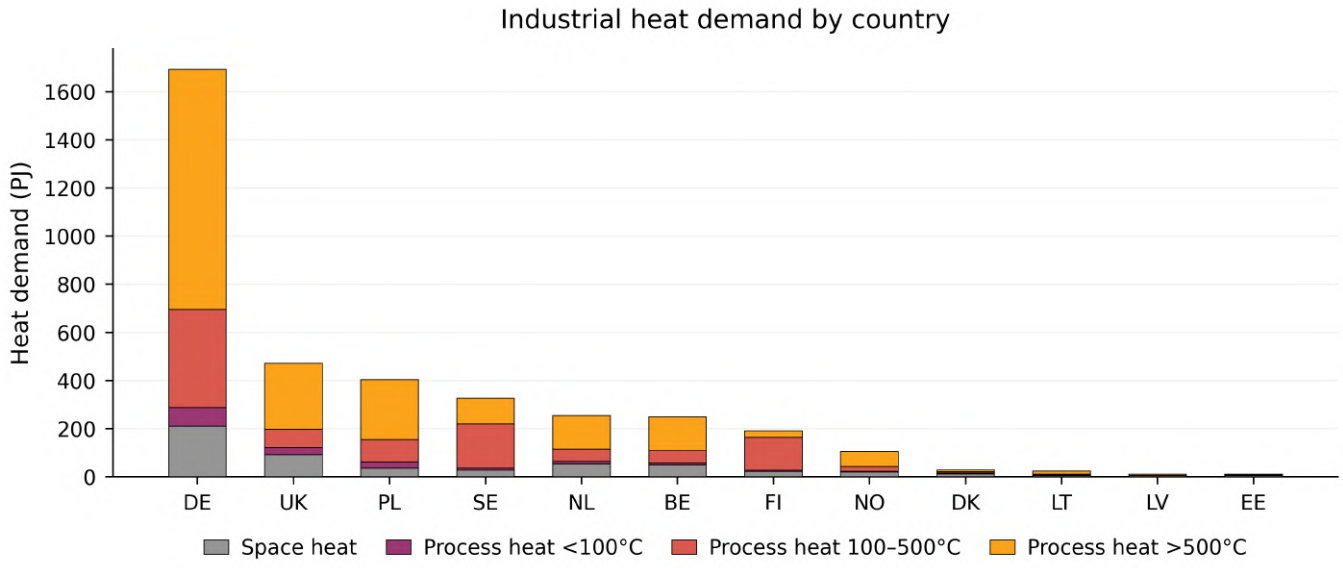

Figure 18: **Industrial heat demand in 2050 by country and temperature level.**

F.3 Exogenous hydrogen demand

Hydrogen demands are derived from the European Hydrogen Backbone[34], which provides country-level hydrogen demand projections by sector for milestone years. We include hydrogen demand in the subsectors fertiliser, steel and industry heat. These demands are implemented as fixed exogenous hydrogen demand in the model. Hydrogen demand for fuel production and high-value chemicals is excluded, as fuel demand and associated hydrogen consumption are determined endogenously.

Regional hydrogen demands are obtained by spatially disaggregating national demand using the same distribution keys as applied for industrial heat demand. Hydrogen demand is specified for the model years 2030, 2040 and 2050.

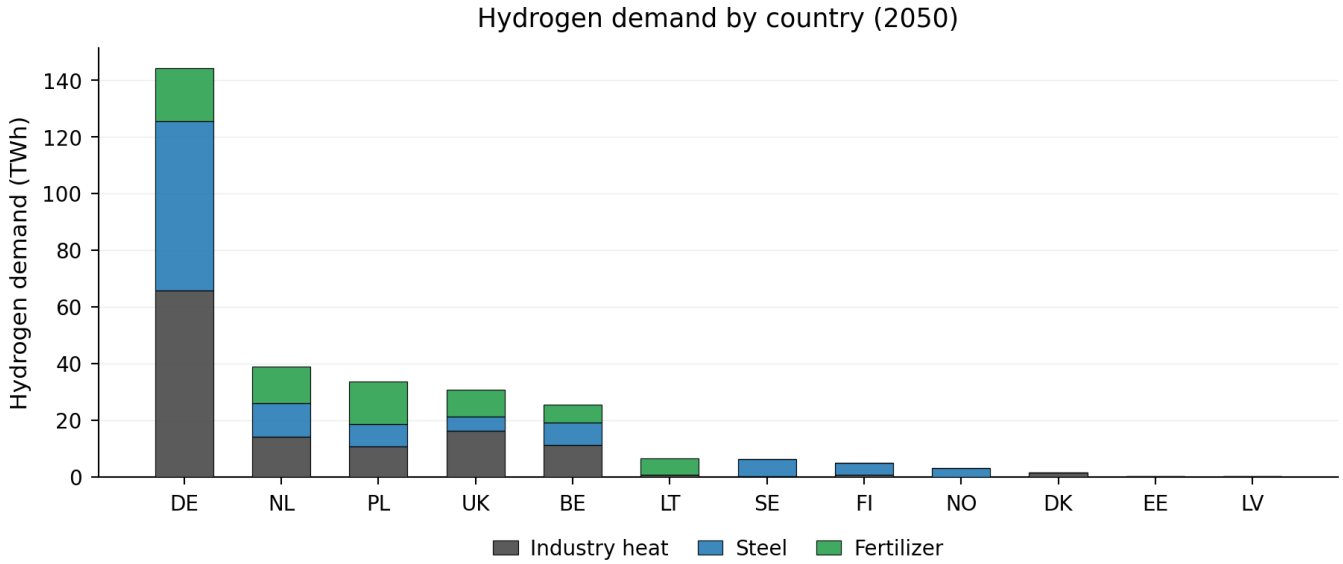

Figure 19: **Exogenous hydrogen demand in 2050 by country and industrial activity.**

F.4 Biomass potential

Biomass resource potentials are derived from the MoPo biomass availability dataset[35]. The dataset provides NUTS3-resolution biomass potentials for Europe across alternative availability scenarios and biomass categories. We use the *medium availability* scenario and exclude primary production from forestry and lignocellulosic energy crops. Included resources comprise forestry and agricultural residues as well as organic waste streams, mapped to the biomass groups used in Balmorel (straw, wood, manure and municipal waste).

Since Norway is not covered at full regional detail in MoPo, Norwegian biomass potentials are supplemented using national statistics. NUTS2-level potentials for straw and wood are downscaled to NUTS3 using regional harvest data[36]. For waste-based streams, potentials are allocated to NUTS3 based on population shares.

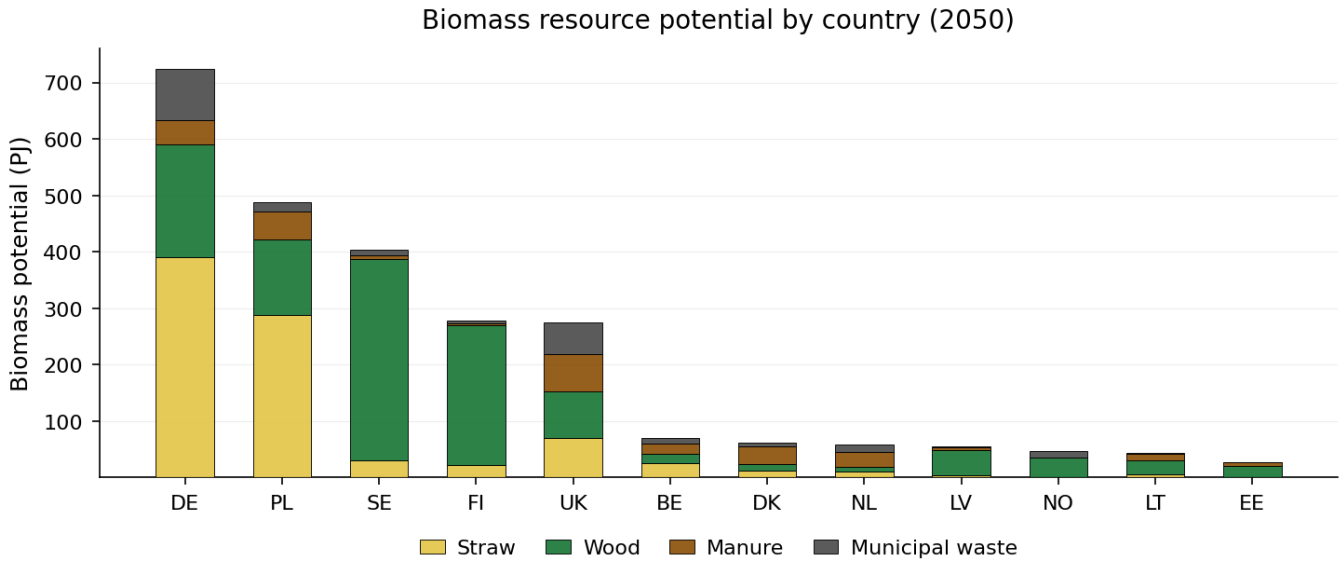

Figure 20: **Biomass resource potential in 2050 by country and modelled biomass group, excluding primary production from forestry and energy crops.**

F.5 Capacity based transmission

Electricity transmission lines and hydrogen and CO_2 pipelines are represented as net transfer capacity between regional centroids with linear bi-directional flows. Investment and fixed operation and maintenance costs are derived from the Danish Energy Agency technology catalogues[25,31]. Capital costs scale with interconnector length and capacity and are split evenly between the connected regions. Routing and construction constraints not captured by centroid links are represented through terrain cost multipliers based on GIS overlays. We apply a multiplier of 1.5 to underwater segments, relative to the affected length, based on values reported by the European Hydrogen Backbone[34]. We also apply a multiplier of 1.25 for segments intersecting mountainous terrain[37,38]. These multipliers are applied uniformly to electricity transmission lines and hydrogen and CO_2 pipelines.

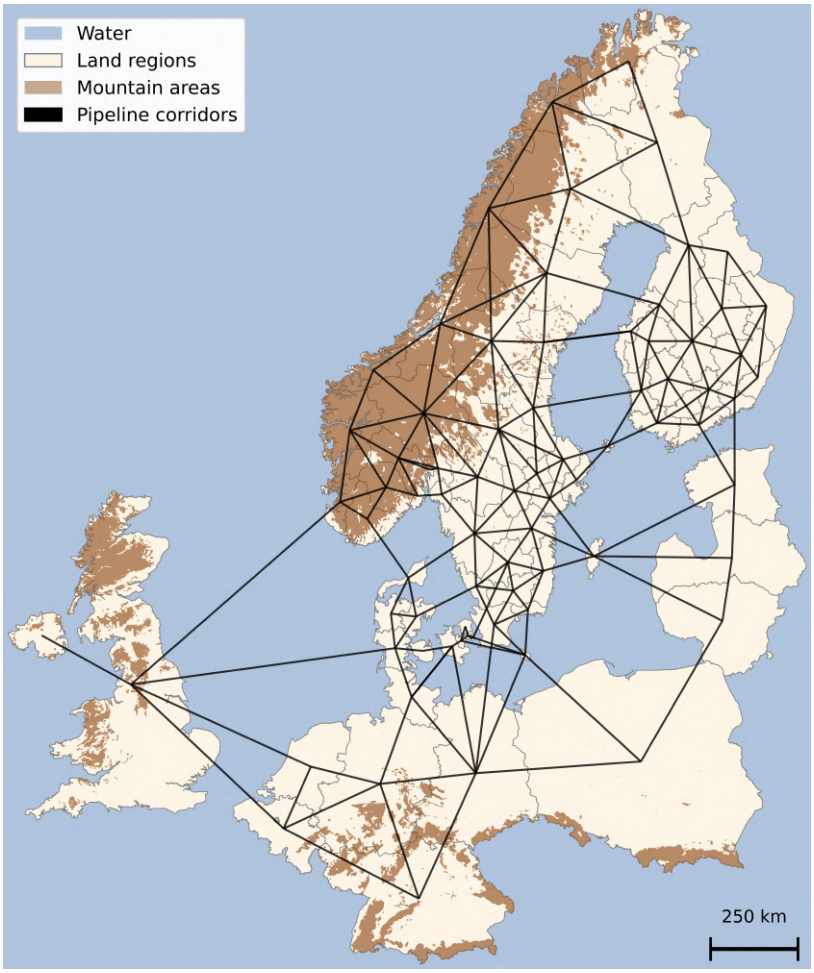

Figure 21: Geographical features used in pipeline cost modelling.

References

1. EA Energianalyse. Analysis of Biomass Prices. Tech. Rep. Danish Energy Agency (2020). URL: https://www.ea-energianalyse.dk/wp-content/uploads/2020/02/1280_analysis_of_biomass_prices.pdf.

2. Galimova, T., Fasihi, M., Bogdanov, D., and Breyer, C. (2023). Feasibility of green ammonia trading via pipelines and shipping: Cases of Europe, North Africa, and South America. Journal of Cleaner Production. URL: https://www.sciencedirect.com/science/article/pii/S095965262303370X. doi: 10.1016/j.jclepro.2023.139212.

3. Galimova, T., Fasihi, M., Bogdanov, D., Lopez, G., and Breyer, C. (2025). Analysis of green e-methanol supply costs: Domestic production in Europe versus imports via pipeline and sea shipping. Renewable Energy. URL: https://www.sciencedirect.com/science/article/pii/S0960148124024042. doi: 10.1016/j.renene.2024.122336.

4. Hampp, J., Düren, M., and Brown, T. (2023). Import options for chemical energy carriers from renewable sources to Germany. PLOS ONE. URL: https://journals.plos.org/plosone/article?id=10.1371/journal.pone.0281380. doi: 10.1371/journal.pone.0281380.

5. Kim, Y.R., Steen, S., Kramel, D., Muri, H., and Strømman, A.H. (2023). Modelling of ship resistance and power consumption for the global fleet: The MariTEAM model. Ocean Engineering *281*. doi: 10.1016/j.oceaneng.2023.114758.

6. Kramel, D., Muri, H., Kim, Y., Lonka, R., Nielsen, J.B., Ringvold, A.L., Bouman, E.A., Steen, S., and Strømman, A.H. (2021). Global Shipping Emissions from a Well-to-Wake Perspective: The MariTEAM Model. Environmental Science & Technology. doi: 10.1021/acs.est.1c03937.

7. European Commission (EC). Reducing emissions from the shipping sector. Tech. Rep. European Commission (EC) (2024). URL: https://climate.ec.europa.eu/eu-action/transport-decarbonisation/reducing-emissions-shipping-sector_en.

8. Pauliuk, S., and Heeren, N. (2020). ODYM - An open software framework for studying dynamic material systems: Principles, implementation, and data structures. Journal of Industrial Ecology *24*. URL: https://onlinelibrary.wiley.com/doi/abs/10.1111/jiec.12952. doi: 10.1111/jiec.12952.

9. Tornatore, C., Marchitto, L., Sabia, P., and De Joannon, M. (2022). Ammonia as Green Fuel in Internal Combustion Engines: State-of-the-Art and Future Perspectives. Frontiers in Mechanical Engineering *8*. URL: https://www.frontiersin.org/journals/mechanical-engineering/articles/10.3389/fmech.2022.944201/full. doi: 10.3389/fmech.2022.944201.

10. Kramel, D., Krey, V., Fricko, O., Maczek, F., Muri, H., and Strømman, A.H. (2026). Maritime sector pathways toward net-zero emissions within global energy scenarios. Scientific Reports. doi: 10.1038/s41598-026-35909-4.

11. Korberg, A.D., Brynolf, S., Grahn, M., and Skov, I.R. (2021). Techno-economic assessment of advanced fuels and propulsion systems in future fossil-free ships. Renewable and Sustainable Energy Reviews *142*. doi: 10.1016/j.rser.2021.110861.

12. Kersey, J., Popovich, N.D., and Phadke, A.A. (2022). Rapid battery cost declines accelerate the prospects of all-electric interregional container shipping. Nature Energy *7*, 664–674. doi: 10.1038/s41560-022-01065-y.

13. Moon, H.S., Park, W.Y., Hendrickson, T., Phadke, A., and Popovich, N. (2025). Exploring the cost and emissions impacts, feasibility and scalability of battery electric ships. Nature Energy *10*, 41–54. doi: 10.1038/s41560-024-01655-y.

14. Mathisen, A., and Skagestad, R. Techno-economic assessment – OCC chain to permanent storage and utilisation. Technical Report D4.4.2 and D4.4.3 EverLoNG Project (2025). URL: https://everlongccus.eu/.

15. Wu, J., Zhang, Y., Jiang, M., Cao, X.E., and Zhang, Z. (2026). Onboard carbon capture, utilization, and storage. Cell Reports Physical Science *7*. URL: https://www.cell.com/cell-reports-physical-science/abstract/S2666-3864(25)00633-2. doi: 10.1016/j.xcrp.2025.103034.

16. Einbu, A., Pettersen, T., Morud, J., Tobiesen, A., Jayarathna, C.K., Skagestad, R., and Nysæther, G. (2022). Energy assessments of onboard CO2 capture from ship engines by MEA-based post combustion capture system with flue gas heat integration. International Journal of Greenhouse Gas Control *113*. URL: https://www.sciencedirect.com/science/article/pii/S1750583621002772. doi: 10.1016/j.ijggc.2021.103526.

17. Visonà, M., Bezzo, F., and d'Amore, F. (2024). Techno-economic analysis of onboard CO2 capture for ultra-large container ships. Chemical Engineering Journal *485*. URL: https://www.sciencedirect.com/science/article/pii/S1385894724014682. doi: 10.1016/j.cej.2024.149982.

18. SEA-LNG. LNG as a Marine Fuel: The Retrofit Investment Opportunity. Tech. Rep. SEA-LNG (2022). URL: https://sea-lng.org/wp-content/uploads/2022/08/VLCC_Retrofit_Investment_Case_Study.pdf.

19. Garbatov, Y., Georgiev, P., and Yalamov, D. (2023). Risk-based retrofitting analysis employing the carbon intensity indicator. Ocean Engineering *289*. URL: https://www.sciencedirect.com/science/article/pii/S0029801823026677. doi: 10.1016/j.oceaneng.2023.116283.

20. Mærsk Mc-Kinney Møller Center for Zero Carbon Shipping. Preparing Container Vessels for Conversion to Green Fuels. Tech. Rep. Mærsk Mc-Kinney Møller Center for Zero Carbon Shipping (2022). URL: https://www.zerocarbonshipping.com/publications/preparing-container-vessels-for-conversion-to-green-fuels.

21. Stopford, M. (2009). Maritime Economics. 3rd ed.. Routledge. ISBN 978-0-415-27558-3.

22. DNV. Maritime Forecast to 2050. Tech. Rep. DNV (2023). URL: https://www.dnv.com/maritime/maritime-forecast-2050.html.

23. Song, Q., Tinoco, R.R., Yang, H., Yang, Q., Jiang, H., Chen, Y., and Chen, H. (2022). A comparative study on energy efficiency of the maritime supply chains for liquefied hydrogen, ammonia, methanol and natural gas. Carbon Capture Science & Technology *4*, 100056. URL: https://www.sciencedirect.com/science/article/pii/S2772656822000276. doi: 10.1016/j.ccst.2022.100056.

24. Smith, J.R., Gkantonas, S., and Mastorakos, E. (2022). Modelling of Boil-Off and Sloshing Relevant to Future Liquid Hydrogen Carriers. Energies *15*, 2046. URL: https://www.mdpi.com/1996-1073/15/6/2046. doi: 10.3390/en15062046.

25. Danish Energy Agency. Technology Data for Renewable fuels. Tech. Rep. 12 Danish Energy Agency (2025). URL: https://ens.dk/en/analyses-and-statistics/technology-data-renewable-fuels.

26. Letoffet, A., Campion, N., Böhme, M., Jensen, C.D., Ahrenfeldt, J., and Clausen, L.R. (2024). Techno-economic assessment of upgraded pyrolysis bio-oils for future marine fuels. Energy Conversion and Management *306*, 118225. URL: https://www.sciencedirect.com/science/article/pii/S0196890424001663. doi: 10.1016/j.enconman.2024.118225.

27. Poulsen, N., Holloway, S., Neele, F., Smith, N.A., and Kirk, K. CO2StoP Final Report: Assessment of CO2 Storage Potential in Europe. Tech. Rep. European Commission Brussels, Belgium (2015). URL: https://energy.ec.europa.eu/publications/assessment-co2-storage-potential-europe-co2stop_en.

28. Goodman, A., Hakala, A., Bromhal, G., Deel, D., Rodosta, T., Frailey, S., Small, M., Allen, D., Romanov, V., Fazio, J., Huerta, N., McIntyre, D., Kutchko, B., and Guthrie, G. (2011). U.S. DOE methodology for the development of geologic storage potential for carbon dioxide at the national and regional scale. International Journal of Greenhouse Gas Control *5*, 952–965. URL: https://www.sciencedirect.com/science/article/pii/S1750583611000405. doi: 10.1016/j.ijggc.2011.03.010.

29. IEAGHG. CO2 storage efficiency in deep saline formations: a comparison of methods. Tech. Rep. 2013/09 IEA Greenhouse Gas R&D Programme (IEAGHG) (2013). URL: https://ieaghg.org/publications/technical-reports/2013-technical-reports/51-2013-09-co2-storage-efficiency-in-deep-saline-formations-a-comparison-of-methods.

30. European Commission (2024). Industrial Carbon Management Strategy. . URL: https://eur-lex.europa.eu/legal-content/EN/TXT/?uri=CELEX:52024DC0062 issue: COM(2024) 62 final Place: Brussels Published: Communication from the Commission to the European Parliament, the Council, the European Economic and Social Committee and the Committee of the Regions.

31. Danish Energy Agency. Technology Catalogue for Carbon Capture, Transport and Storage. Tech. Rep. Danish Energy Agency Copenhagen, Denmark (2023). URL: https://ens.dk/en/analyses-and-statistics/technology-data-carbon-capture-transport-and-storage.

32. Rehfeldt, M., Fleiter, T., and Toro, F. (2018). A bottom-up estimation of the heating and cooling demand in European industry. Energy Efficiency *11*, 1057–1082. URL: https://doi.org/10.1007/s12053-017-9571-y. doi: 10.1007/s12053-017-9571-y.

33. Pezzutto, S., Zambotti, S., Croce, S., Zambelli, P., Garegnani, G., Scaramuzzino, C., Pascual Pascuas, R., Zubaryeva, A., Haas, F., Exner, D., Mueller, A., Hartner, M., Fleiter, T., Klingler, A.L., Kuehnbach, M., Manz, P., Marwitz, S., Rehfeldt, M., Steinbach, J., and Popovski, E. (2018). Hotmaps Industrial Sites: Industrial Database (EU28). Hotmaps Project. URL: https://gitlab.com/hotmaps/industrial_sites/industrial_sites_Industrial_Database.

34. van Rossum, R., Jens, J., La Guardia, G., Wang, A., Kühnen, L., and Overgaag, M. European Hydrogen Backbone: A European Hydrogen Infrastructure Vision Covering 28 Countries. Report European Hydrogen Backbone (2022). URL: https://ehb.eu/files/downloads/ehb-report-220428-17h00-interactive-1.pdf.

35. Louis, J.N., Kiviluoma, J., and Lindroos, T.J. (2024). Biomass availability at NUTS3 level for modelling European energy system with 3 future scenario. Zenodo. URL: https://zenodo.org/records/14506624. doi: 10.5281/zenodo.14506624.

36. Ogner Jåstad, E., Folsland Bolkesjø, T., Rørstad, P.K., Midttun, A., Sandquist, J., and Trømborg, E. (2021). The Future Role of Forest-Based Biofuels: Industrial Impacts in the Nordic Countries. Energies *14*, 2073. URL: https://www.mdpi.com/1996-1073/14/8/2073. doi: 10.3390/en14082073.

37. Tumara, D., Uihlein, A., and Hidalgo Gonzalez, I. Shaping the future CO2 transport network for Europe. Tech. Rep. Joint Research Centre (JRC), European Commission (2024). URL: https://publications.jrc.ec.europa.eu/repository/handle/JRC136709. doi: 10.2760/582433.

38. Pershad, H., Harland, K., Stewart, A., Slater, S., Race, J., Hunt, P., and Zakkour, P. Development of a global CO2 pipeline infrastructure. Tech. Rep. IEAGHG (2010). URL: https://ieaghg.org/publications/development-of-a-global-co2-pipeline-infrastructure/.